Transfer Entropy Analysis of the Interactions of Flying Bats

Nicholas B. Orange

Thesis submitted to the Faculty of the
Virginia Polytechnic Institute and State University
in partial fulfillment of the requirements for the degree of

Master of Science
in
Engineering Mechanics

Nicole Abaid, Chair
James Hanna
Shane Ross
Rolf Müller

May 4, 2015
Blacksburg, Virginia

Keywords: Transfer Entropy, Animal Behavior, 3D Tracking

Transfer Entropy Analysis of the Interactions of Flying Bats

Nicholas B. Orange

(ABSTRACT)

In this document, a low-cost, portable, non-invasive method of collecting the 3D trajectories of flying bats is first presented. An array of commercially available camera and light components is used alongside a number of well-established calibration and triangulation techniques to resolve the motion of agents through a 3D volume. It is shown that this system is capable of accurately capturing the bats' flight paths in a field experiment. The use of non-visible illumination ensures that a natural cave environment is disturbed as little as possible for behavioral experiments.

Following is a transfer entropy analysis approach applied to the 3D paths of bats flying in pairs. The 3D trajectories are one-dimensionally characterized as inverse curvature time series to allow for entropy calculations. In addition to a traditional formulation of information flow between pair members, a path coupling hypothesis is pursued with time-delay modifications implemented in such a way as to not change the Markovianity of the process. With this modification, trends are found that suggest a leader-follower interaction between the front bat and the rear bat, although statistical significance is not reached due to the small number of pairs considered.

This work is supported by the National Science Foundation under grant EEC-1342176 and by the Institute for Critical Technology and Applied Science at Virginia Tech.

Acknowledgments

I would like to thank my committee members Dr. Hanna and Dr. Ross for helpful discussions; Dr. Müller for providing experimental support, lab resources, and biological expertise; the Shandong University Virginia Tech International Laboratory and its members for experimental support, expertise, logistics, and camaraderie; and my advisor Dr. Abaid for exceptional knowledge and patience.

Contents

List of Figures

List of Tables

Chapter 1

A Novel, Low-Cost Near-Infrared Camera System for the 3D Tracking of Bat Flight in the Field

1.1 Introduction

Tracking the three-dimensional (3D) paths of flying agents is a well-established problem that has been extensively tackled with multi-camera reconstruction in a variety of cases from laboratory insects[1] to the tandem flights of cliff swallows in the wild[2]. In these cases, sufficient day-time light or controlled laboratory lighting makes computer vision detection of these agents possible. With nocturnal animals, such as bats, collecting data in a non-laboratory environment creates an additional challenge: lack of day-time illumination. Unfortunately, this challenge cannot be solved simply by using portable, visible-spectrum lights without influencing animal behavior. Many species of bats are capable of seeing a range of visible light [3] and using it for orientation [4, 5]. Given this, it would be disruptive to flood a dark space or cave with visible-spectrum light, as this could lead to upset or unnatural behavior, making any results unrepresentative of the natural state. Therefore, a non-visible light solution is necessary if maintaining the sanctity of the natural behavior and environment is a priority.

Thermal optical systems are the primary non-visible solution addressing this issue and have been used successfully to track bats in dense swarms [6] and evaluate wingbeat patterns[7]. Unfortunately, obtaining these systems involves a significant cost, as thermal cameras capable of the high-resolution, high-speed capture necessary to resolve the motion of bats often cost between $10,000 and $80,000 dollars per camera, based on personal discussions with established thermal camera companies. This leaves a unique role to be filled by a system capable of comparable non-intrusive 3D capture performance with a more accessible cost

figure.

To fill this role, a near-infrared solution is developed. Near-infrared light occupies a small spectrum between short-wave infrared and visible red, typically referring to 650-1050 nm wavelength light [8]. For this application, the low-frequency end of this spectrum (950 nm wavelength light) is chosen, which is typically invisible to the human [9] and the bat eye [10], but behaves similarly to visible light. Most importantly, modern digital image sensors can detect near-infrared light, though it is conventionally blocked by infrared filters within the lens to better reflect the spectral response of the human eye [11]. By fully utilizing the spectral range of commercially available digital cameras, one can exploit the low cost of this equipment to achieve a novel solution to non-invasive tracking that reduces cost and, as an added benefit, is extremely portable. To the knowledge of the author, this system is the first of its kind.

The novelty of this camera system lies in the hardware specifications and setup, rather than the data processing or calibration strategies, which are based on well-founded 3D tracking concepts and open-source toolboxes. For this reason, this chapter will detail the selection and arrangement of the hardware components and briefly discuss the process of turning the raw video data into 3D paths.

The system's performance is demonstrated in a mountain cave near Jinan, China. This data collection was part of a larger project to analyze the interactions of bats in swarms or in pairs. The population of bats in the cave were primarily of the genus *Myotis* and would leave the roosting area of the cave center to feed on insects every night immediately after sunset. 3D data was collected in a hallway-shaped section of the cave near the exit, which provided a good environment for generating long, distinguishable paths for the entropy analysis shown in the next chapter. It is found that the camera system performed as expected and was able to accurately resolve the 3D paths of the bats that flew through the volume of interest.

1.2 Hardware Selection

In order to effectively capture the motion of small, fast moving objects (bats), it was necessary to use cameras with high spatial resolution and frame rate abilities. The GoPro Hero 3+ Black Edition proved to be an affordable and effective option for meeting those requirements while shooting at 1920×1080 pixel resolution and 60 Hz. The high resolution allowed for a usable range of roughly 40 meters, inside of which a well-lit bat would be easily visible to a camera. Given that the bats represented in the data flew with a velocity up to 9 m/s, a 60 Hz capture rate ensured that each bat traveled no more that 15 centimeters between frames. In addition to these metrics, the GoPro cameras were preferable due to their small size, light weight, and waterproofing cases, which made them ideal for field work.

In order to utilize non-visible light, the original GoPro lenses are replaced with IR-Pro IRP202 Hybrid lenses[12], which permit the passage of a full spectrum of infrared, visible,

Figure 1.1: Infrared vision image of the field site in Jinan, China. The purple hue represents the 950 nm near-infrared wavelength interpreted by the GoPro camera's IR-sensitive hardware.

and ultraviolet light to the camera sensor while maintaining similar geometry. The stock GoPro lens has a 2.92 mm focal length and a field of view of 123 degrees, while the IR-Pro lens has a 2.5 mm focal length with a field of view of 134 degrees. Given that the IR-Pro lenses are designed to replace the original lens, the replacement process was as simple as unscrewing the original lens and screwing in the IR-Pro replacement, though manually focusing the new lens is necessary. The final product here is a full spectrum digital camera with the performance of the original GoPro. Used in conjunction with Sima SL-100IR 950 nm LED array illuminators, a complete non-visible lighting and capture system was attained. A sample image of the field site illuminated with 950 nm light taken with a near-IR-modified GoPro camera is shown in Figure 2.1.

It should be noted that both the cameras and illuminators are powered by internal, rechargeable lithium-ion batteries, meaning that all components can function for a reasonable duration in the field. The GoPro cameras were found to record continuously for around 1.5 hours, while the illuminators would begin to dim after 2.5 hours. In order to achieve longer recording times, small, external 2200 mA USB power supplies could be connected to the cameras to double their life.

For data storage, each GoPro's built-in SD card slot is used to write to a 32 Gb SD card (SanDisk Ultra Micro SDHC). At 1080p and 60 fps, 32 Gb allowed us to record for roughly 2.5 hours uninterrupted. This internal storage capability gave a significant advantage in portability by making additional capture hardware unnecessary.

Additional equipment needed for a functional setup included lightweight SLIK F143 tripods, a Samsung SM-T320 Galaxy Tab Pro tablet, and a 5 mW green laser pointer. By combining various accessory mounting pieces with basic hardware, tripod mounts were constructed that

Figure 1.2: A fully constructed tripod includes one modified GoPro camera, one illuminator, and one external battery.

Figure 1.3: All camera system components fit into a 42cm × 33.1cm × 17.4cm pelican case for transport.

would securely hold, in any orientation, a GoPro camera, illuminator, and battery pack. These snapped into the tripods, providing a simple, lightweight structure for each camera. A single camera setup on a tripod is shown in Figure 1.2. The tablet was needed to preview each camera's vision in order to ensure proper alignment. This was done by connecting the official GoPro app installed on the tablet to each camera's built-in Wi-Fi network. The laser pointer was capped with a piece of cellophane tape to create an approximate point light source and was used in the later steps of calibration.

By carefully selecting the cost-effective, portable components described, a fully functional six camera setup with 15 illuminators (including an additional back-up camera, not including tripods) could be fit into a 42cm × 33.1cm × 17.4cm Pelican case (Model 1450) for safe transport, shown in Figure 1.3. The total cost of the full system with all components is only $4539 and weighs a total of 12 kg, including tripods. This mass figure makes the system highly mobile, such that a single person can comfortably carry and setup all necessary components.

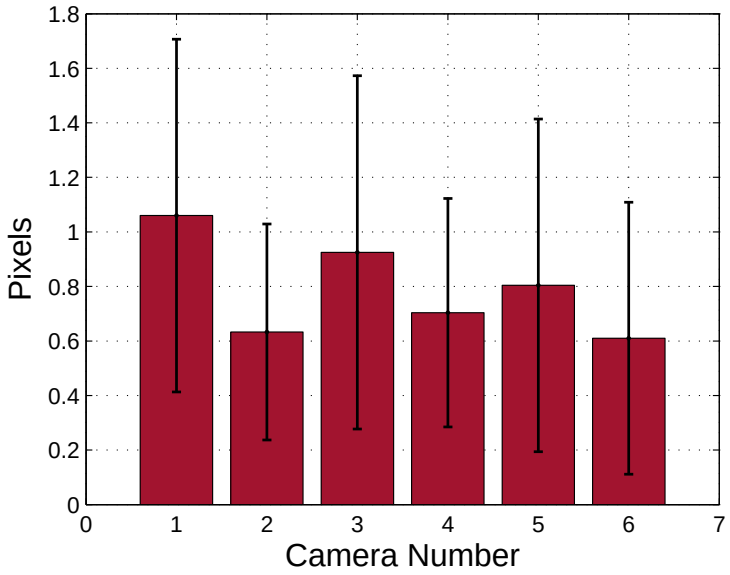

Figure 1.4: Mean 2D reprojection error for the six camera setup computed by the Svoboda multi-camera self-calibration toolbox. Error bars show one standard deviation.

1.3 Setup and Calibration

Assembly, placement, calibration, and systems check take approximately one hour. At the Jinan field site, the cameras were arranged in a rectangular pattern, allowing the capture of the 12m × 6m × 5m hallway formed by the cave, while maximizing the orthogonality of the camera lines of sight. Because the GoPro cameras have no method of external syncing, temporal syncing was performed by flashing the laser pointer in view of all cameras and extracting the exact frame of the flash after the recording. This method creates a timing error of +/- 0.5 frames, which is manageable given the high frame rate. It should be noted that this temporal sync issue can be addressed by syncing the audio tracks, which sample at a much higher rate of 44 kHz, and interpolating tracked 2D paths to achieve sub-frame accuracy. This effectively eliminates the timing error. This process may or may not be necessary to achieve good results depending on the velocity of the object being tracked and the frame rate used. In this project, sub-frame interpolation was not needed to achieve positive results.

3D calibration was performed in accordance with the Svoboda Multi-Camera Self-Calibration MATLAB toolbox [13]. The taped laser pointer was walked through the capture volume and recorded on all cameras. After recording, the sets of 2D points from each camera view were used to extract the extrinsic 3D information of the camera positions. An assessment of calibration success is made by the 2D reprojection error of the tracked laser points[14]. For this camera system, the cameras were calibrated in four different configurations and it was consistently found that the mean 2D reprojection error over the six cameras was less than

Figure 1.5: Example plot of image processing and 2D tracking results from verified automatic method in MATLAB. The green and orange paths represent the time histories of the leading and following bats respectively.

0.8 pixels. In particular, for the camera setup in the exemplary experiment discussed in this chapter, the statistics for the 2D reprojection error from each camera is given in Figure 1.4; the mean 2D reprojection error over the six cameras in this case is 0.77 pixels.

As a component of this calibration, an intrinsic 2D distortion adjustment is made by the Caltech Camera Calibration MATLAB toolbox [15]. This adjustment is made for each camera lens separately and is fed into the 3D Svoboda calibration by setting the intrinsic camera properties. This step is necessary to resolve the significant distortion present in wide-angle lenses. The final component of calibration is relating the arbitrarily scaled environment produced by the Svoboda toolbox to real-world dimensions[14]. This requires a single, physical length scale to apply to the final 3D environment, which can be obtained from the triangulation of a set of real points, or by measuring the distances between the cameras. In this setup, the distances between cameras was used for this scaling.

1.4 Processing

Image processing is performed after the data is collected using a background subtraction method. In this method, a representative average image is subtracted from each frame. Pixel groups that differ significantly from the background are cut out with a binary mask and traced with a Moore-Neighbor algorithm from the MATLAB Image Processing toolbox. The presence of a bat is determined by comparing each pixel group with nearby candidates (a set of similar pixel groups within a certain distance) in the frames before and after and, from

these, determining if a valid time evolution of the group is present based on the smoothness of the path generated by the pixel group moving between the three frames. This use of motion information allows for both a double-check of the validity of a detected object, as well as the distinction of high-level noise from dimly-lit bats, which can be necessary if lighting is insufficient or inconsistent.

With the 2D locations of every bat determined, any number of 2D/3D tracking strategies can be implemented. With consistent and continuous 2D data, a fully automatic system can be implemented, following the well-founded, well-documented techniques in[16, 17, 18, 19]. If less-than-desirable lighting conditions exist, the results of 2D tracking may become inconsistent, leading to problems with 3D correlation depending on the technique employed. In this situation, a verified automatic or purely manual tracking approach may be deemed best.

A user-verified automatic 2D tracking method that merged with a simple 3D reconstruction algorithm was elected for this implementation. Within a user-interface, a bat is selected for tracking from one camera view and a 2D extrapolative motion tracker extracts the path of the bat while the user watches the progress and makes corrections as necessary. This tracking is performed on data from all cameras with a view of the bat. An example of this process from one camera view is shown in Figure 1.5. The 3D reconstruction algorithm collects the 2D information from each camera and projects the lines of sight into 3D space. To best resolve the final 3D position of the converging lines of sight, a least squares regression formulation is used to minimize the orthogonal distance of each line from the final 3D point. Additionally, though the intrinsic distortion of the lens is adjusted for, the outer edges of the camera view are still to be considered less reliable. As such, the regression includes weighting that considers the centered-ness of a camera view.

After tracking and triangulation, a first-order locally weighted smoothing method is applied to the 3D path data. This method eliminates residual tracking error and oscillatory motion of the bat's centroid resulting from wing beat, while best considering the fundamental linear momentum of a flying bat.

For this project, all image processing, 2D tracking, 3D reconstruction, and analysis were performed in MATLAB. The Caltech toolbox provided routines for distortion adjustment and MATLAB toolboxes and built-in functions were used in tracing, smoothing, and minimization. The remainder of the processing was performed with custom MATLAB codes.

1.5 Results

10 pairs of bats flying in proximity were collected, a sample of which is shown in Figure 2.2. As a complete validation of the reconstruction, the inverse problem is performed and the 3D points are reprojected back onto the camera views. Samples of this validation in two camera views of a single path are shown in Figure 1.7. The mean reprojection error

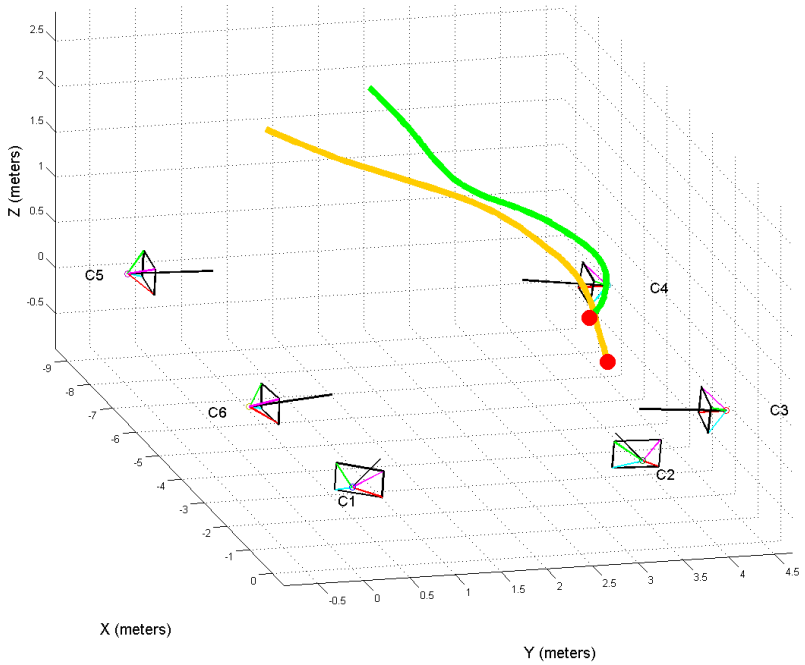

Figure 1.6: Plot of final 3D path reconstructions of two bats flying as a pair. Camera positions, orientations, and fields of view are also shown.

of these samples, calculated between the smoothed 3D points and the 2D tracked points in both cameras, is 5.01 pixels, a reasonable figure when considering the high resolution and wide-angle distortion of the cameras. With this validation it is determined that the system is capable of accurately tracking the 3D location of bats within the collection volume.

1.6 Discussion

Successful experimental design is centered around the use of reliable, accurate equipment for data collection which often creates a necessity for science-grade or professional hardware. The cost advantage of the system described in this chapter fundamentally lies in its use of commercially available, consumer-grade hardware rather than science-grade hardware. This factor allowed the cost goals of the project to be met. The use of GoPro cameras had additional advantages in that they are very small, very light, and self-contained, making the final system extremely efficient for field work. However, some noticeable drawbacks to using the GoPro cameras exist which are quintessential issues with consumer-grade hardware in general. These drawbacks are addressed in the following discussion.

The most significant drawback is the lack of synchronization control or an external trigger, which creates a temporal error of $\pm$ 0.5 frames, leading to increased 3D error as the velocity of the tracked object increases. It was discussed how this can be addressed by using the

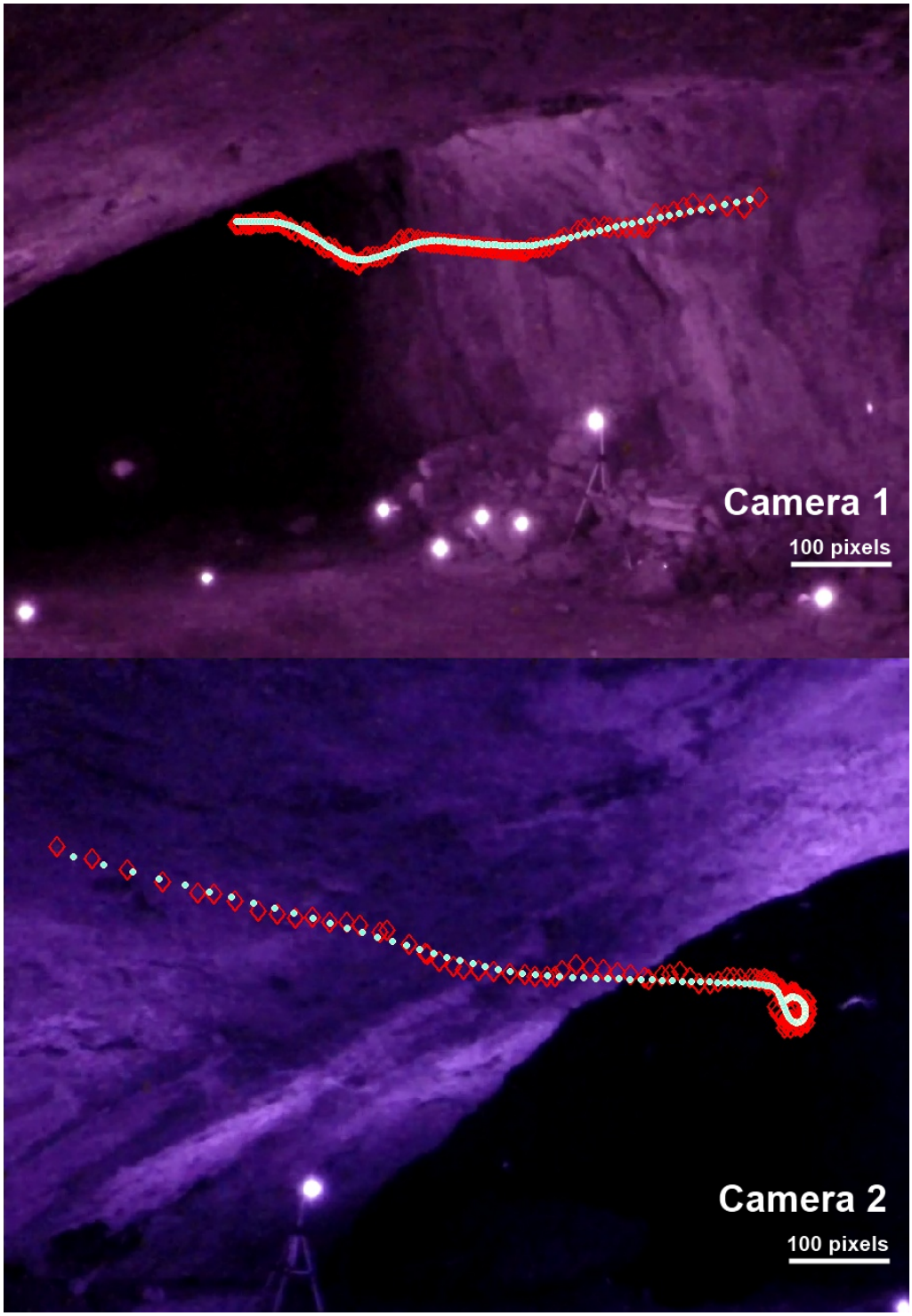

Figure 1.7: Example plot of final 2D reprojection validations. Red diamonds indicate 2D tracked points, and white circles final 3D points. The mean reprojection error is 5.01 pixels. Source images have been cropped to better show path points.

camera audio tracks to sync with sub-frame accuracy, but this issue would be entirely avoided with an external trigger, a standard feature in most science-grade cameras and even some consumer-grade cameras.

Lossy compression presents another concern. The GoPro camera output is a .mp4 codec which uses compression to achieve reasonable file sizes for extended high-definition recording. This compression can result in information loss either by reducing the overall signal to noise ratio of the data or by smoothing out small, non-distinct pixel groups that may represent bats. In general, this is not an issue in well-lit, high-contrast environments, but it can create detrimental effects when filming in low-light conditions. This places an added importance on achieving good lighting conditions with near-infrared illumination. If proper lighting is unattainable, a camera capable of uncompressed video output should be used to ensure the best possible result.

Lastly, it was found that the GoPro cameras were occasionally subject to shutting down as a result of high temperatures reached during long recordings. This issue was encountered primarily in the lab during testing, where ambient airflow was not as present. It was determined that reducing the internal battery load is the best method for avoiding this problem, which can be done by turning off Wi-Fi functionality or using an external battery pack. The next generation of GoPro cameras available as of 2015 will likely not be subject to this issue, though this has not been confirmed.

By using commercially available GoPro cameras, it is inevitable that some amount of accuracy, functionality, and reliability is traded for cost savings and improved portability. This represents a typical and rather intuitive issue with equipment selection. In this case, a lack of external triggering, compression concerns, and over-heating issues were encountered. However it was shown that these issues can be resolved and 3D tracking results can be achieved that are comparable to the results of systems with 10 times the cost. This point serves to suggest that commercial hardware, especially commercial video cameras, shouldn't be ignored when cost metrics are of importance and sufficient time for system testing is available.

Potential ultrasonic signature of the system is also addressed. Because bats use ultrasonic pulses to echolocate, any ultrasonic noise created by electronics or other sources would be unacceptable for a non-invasive field setup. To ensure that this system was not producing an ultrasonic signature, a Wildlife Acoustics Song Meter SM2BAT+ ultrasonic recorder with a SMX-UT microphone was used to monitor the system components while reproducing a typical data collection process. Waveform data was analyzed in MATLAB and it was confirmed that no ultrasonic noise was being generated.

The SLIK F143 tripods used are designed to be lightweight rather than to maximize stability and rigidity. Indeed, heavier, professional tripods can provide a sturdier base for the cameras which may better prevent error created by post-calibration movement. However, there a number of factors that reduce this advantage of heavier tripods and support the use the existing lightweight tripod setup. Because of the Svoboda calibration method used, no physical contact with the camera is made after the calibration phase until the end of

the recording period. This means that, excluding an extreme scenario where a camera is deliberately jostled or struck by a bat, only infinitesimal movement of the camera can occur, possibly as a result of temperature changes or wind pressure. These infinitesimal movements would create error only noticeable on systems where less than sub-pixel error is critical; it would not significantly effect the output of this system. As such, the use of lightweight tripods was found to be prudent.

There are some routes to consider towards improving the performance of this system. Most viable is the potential use of rectilinear (flat) lenses which would decrease the field of view of the camera but entirely eliminate lens distortion, which is the biggest contributor to spatial error. With some brief testing of the modified fields of view and adjustments to setup geometry, this small change would likely show a large reduction in error. Conveniently, IR-Pro has recently made available a similar full spectrum GoPro lens product that is fully rectilinear[20].

Another potential improvement is increasing the capture rate to 120 Hz or more, as made possible by the newest generation of GoPros or other cameras. An increased capture rate would be most helpful for the implementation of an automatic tracking algorithm applied to dense groups, where smaller time steps can help better distinguish the motion of individuals[18]. Increased capture rate would also provide more samples of any given 3D trajectory, however this proves to be rather non-valuable. Based on the wingbeat rate estimated from the video data and the smoothness of the paths observed during maneuvers, there seems to be a functional limit as to how sharp a bat can turn, and a 60 Hz capture rate is sufficient for even the most drastic motion observed. If a higher sample rate is desired, a spline fit through the 60 Hz data can be resampled for a sufficiently identical result.

Finally, a brief discussion of non-visible illumination is warranted. Working with near-infrared lighting is uniquely difficult in that it is absolutely critical to the system performance while being total invisible by conventional means. Given this, it is essential to gain experience with infrared illumination before attempting to collect data in the field. If possible, the exact film site should be visited beforehand and testing should be done to check that objects moving through the zone of interest are effectively illuminated. A modified GoPro, monitored with a tablet, serves as an effective means for surveying the illuminated space. More powerful illuminators than the small illuminators used in this paper should be considered for filming in larger spaces. If shooting against a dark background is possible, this improves results significantly.

Chapter 2

Transfer Entropy Analysis of Leader-Follower Interactions in Flying Bats

2.1 Introduction

Bat navigation and group dynamics represent a rich subject area of potential study. Highly evolved collective motion utilizing active sensory echolocation creates numerous avenues of exploration that can benefit our understanding of swarming mechanics, consensus modeling [21], collective robotics [22, 23], and optimization strategy [24, 25]. In recent years, significant progress has been made in capturing the fundamental phenomena involved in these natural systems, as is detailed below.

Evidence of frequency modulation capabilities [26, 27] clearly show that bats have evolved echolocation behaviors to mediate their interactions with conspecifics. Similar behaviors include vocalization cessation [28], which can allow bats to switch from active to passive sensing, and even offensive jamming during feeding competition [29]. With these behaviors in mind, it is clear that bats act differently together than alone and, in many situations, this can benefit their survival.

Modern agent-based swarm modeling and consensus modeling can provide some additional insight towards understanding the complexity of bat group motion. Particularly salient lessons are the importance of goal-orientation and leadership [30, 31]. While we can observe and understand the navigational goals of bat agents, such as feeding or energy conservation, clearly defining navigational leadership roles, even relative ones, in real bat systems is a challenge. Particularly, a quantitative assessment of navigational leadership within bat groups appears to be an entirely untouched area of study. Given the broadcast nature of bio-sonar, the active sensing of one individual can directly influence the motions of others, making the

directionality of leadership unclear.

In this chapter, a contribution is made towards the understanding of navigational leadership in bats. The exploration of this area is refined by focusing efforts on pairs of bats and pursuing a method of analysis involving the application of transfer entropy.

Transfer entropy is a measure of directional information transfer between random processes. Centered around the concept of Shannon entropy [32, 33], transfer entropy allows simultaneous time series to be assessed in terms of the strength and direction of their coupling [34, 35, 36] by measuring the reduction in uncertainty of one time series when knowledge of the other time series is gained. With rapidly increasing interest, transfer entropy has been successfully applied to a large variety of subject areas including neuroscience [37], economics [38], and social media [39]. Particularly, entropy approaches have been developed for assessing animal behavior [40, 41, 42] and information transfer in swarm models [43].

This wide base of work provides an excellent foundation with which to structure a novel approach to the problem of bat navigational leadership. The core concept here is to apply a transfer entropy analysis to characteristic kinematic time series representing the 3D paths of bats flying in pairs. Differing values of directional transfer entropies between members of each pair are expected to function as good indicators of potential leadership roles.

3D trajectories of wild bats flying in pairs are collected and examined; qualitative evidence is found that a coupling between their paths often appears. Given that the cave environment site of data collection is controlled to be consistent through time and that a large variety of path shapes are displayed, it is highly compelling that the paths of the bats within a pair are qualitatively similar. Thus, the hypothesis of a path coupling within pairs is conceived. A cursory examination of the simultaneous inverse curvature plots also supports this hypothesis. Strong curvature equivalency can be detected in many pairs, though the equivalency occurs across a significant time delay, a phenomena that is thoroughly described later in this chapter.

With these observations, it is believed that strong interactions exist within the bat pairs and that this interaction is demonstrated by path shapes. Though the direction and magnitude of path coupling was unclear initially, it is hypothesized that one can resolve these properties using a transfer entropy analysis of the inverse curvature time series or other kinematic metrics, which is explored in this work.

After applying a well-founded adjusted entropy formulation that allows for the capture of the time delay inherent with path coupling, directional transfer entropy values are calculated for each pair. Higher information transfer is found from the bat flying in front to the bat flying in the rear when the path coupling time delay is considered, as compared to all other entropy transfer figures (front to rear with no time delay, rear to front, and random pair shuffling); these trends fail to reach statistical significance due to the small number of bat pairs considered. Nevertheless, this result provides evidence that relative spatial positioning plays an important role in navigational leadership and quantifies the amount of path coupling

Figure 2.1: Infrared vision image of the field site in Jinan, China. The purple hue represents the 950 nm near-infrared wavelength interpreted by the GoPro camera's IR-sensitive hardware.

that occurs within interacting pairs of flying bats.

2.2 Data Collection and Preparation

As detailed in the previous chapter, data is collected in a mountain cave in Jinan, China, in which, a long, hallway-like portion of the cave was found to be ideal for tracking continuous paths of small groups of bats. A 3D near-infrared camera system was setup and calibrated to obtain the 3D paths of bats along a 12 meter portion of the cave "hallway." This camera system consisted of 6 modified GoPro cameras filming at 1920×1080 resolution and 60 Hz. 950 nm LED arrays were used to create artificial illumination that is invisible to the natural eye, but able to be detected by the modified camera hardware, as shown in Figure 2.1.

Intrinsic camera calibration was performed with the Caltech Camera Calibration Toolbox for MATLAB[15] and spatial calibration with the Svoboda Multi-Camera Self-Calibration method[13]. Image processing and 3D reconstruction were performed with custom MATLAB codes following well-established triangulation techniques. A detailed description of the experimental setup and data processing can be found in the previous chapter.

Ten pairs of bats were tracked as they flew through the volume. Pairs were selected if two bats coincided in the tracking volume for 50 or more frames and no other bats were in the tracking volume throughout the duration of the pair's flight. The purpose of this measure was to best enforce that the two bats being tracked were only interacting with each other, rather than surrounding bats. Some bats flew directly through the hallway, while others made a complete turning maneuver and returned the direction they came. In all cases, the

Table 2.1: General flight data of bat pairs.

Pair	Flight path type	Front bat avg vel ($\frac{m}{s}$)	Rear bat avg vel ($\frac{m}{s}$)	Avg separation (m)	Δt (s)
1	Straight through	6.28	6.16	2.94	0.48
2	Straight through	5.05	5.93	2.93	0.49
3	Turn back	3.11	2.60	1.13	0.44
4	Straight through	4.00	4.74	4.37	0.92
5	Straight through	4.98	5.48	2.49	0.45
6	Straight through	4.72	5.26	3.48	0.66
7	Straight through	5.76	5.01	3.16	0.63
8	Straight through	6.58	5.90	3.37	0.57
9	Turn back	4.44	5.49	2.69	0.49
10	Straight through	5.33	3.78	3.05	0.81

first bat to enter the tracking volume was labeled as the front bat, and the other, the rear bat. Details of the tracked paths are shown in Table 2.1.

The 3D path points of each bat were extracted from the video data and a first-order locally weighted smoothing method was applied. This method eliminates residual tracking error and oscillatory motion of the bat's centroid resulting from wing beat, while best considering the fundamental linear momentum of a flying bat. A sample of these 3D paths is shown in Figure 2.2.

In order to perform a transfer entropy analysis of these pairs, it was necessary to generate one-dimensional time series from three-dimensional path data. A number of potential metrics for representing 1D time series were considered; it was found that an inverse radius of curvature metric was best for a number of reasons. Primarily, a curvature-based time series would be reflective of a bat's steering and thereby provide a good depiction of the 3D navigation of the bat pairs. Secondarily, an absolute inverse radius of curvature formulation would ensure the data remains positive and close to zero, making a logarithmic binning strategy possible. Finally, inverse radius of curvature was sufficiently time-varying to be a good candidate for entropy analysis without being as chaotic as a higher-order metric, such as kinematic jerk. As an additional reason, curvature-based metrics are well-founded, in that they are frequently used to assess the motion of interacting agents, such as in the study of laboratory insects [1]. Nevertheless, entropy analyses are performed on other metrics, as presented in the discussion section of this chapter.

To extract the inverse radius of curvature time series, a third-order spline is fit through the 3D path points and re-sampled in time at the desired sample rate, if different than the original 60 Hz. The spline is then differentiated twice to generate 3 component velocity ($\mathbf{v}$) and acceleration ($\mathbf{a}$) vector data at each point. Using Equation (2.1), one can determine the vector of normal acceleration ($\mathbf{a_n}$), which is then used by Equation (2.2) to determine the inverse radius of curvature ($1/R$). Figure 2.3 shows sample plots of the calculated inverse curvature time series pairs.

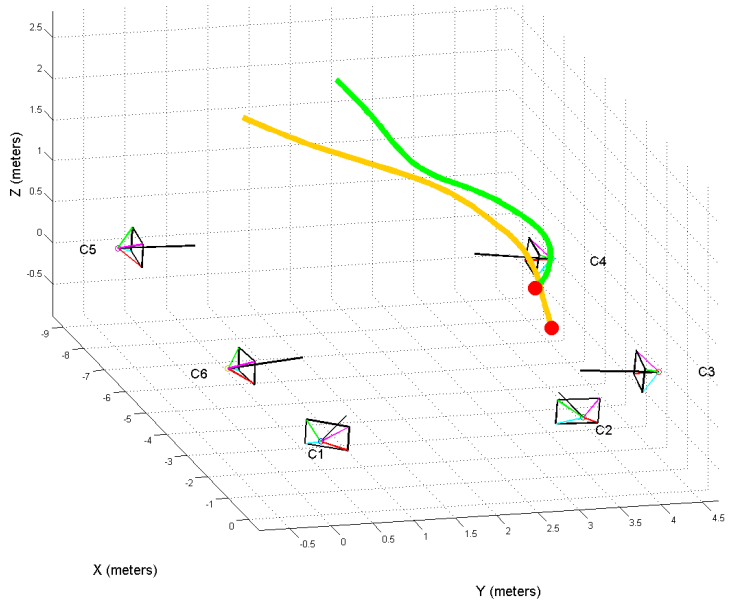

Figure 2.2: A 3D reconstruction of the complete paths made by Pair 2. The green path represents the front bat and the yellow path the rear bat. The 6 camera positions, orientations, and fields of view are also represented. Note the similarity of the path shape. Other pairs display comparable similarity.

$$\mathbf{a_n} = \mathbf{a} - \mathbf{a_t} = \mathbf{a} - \frac{\mathbf{a} \cdot \mathbf{v}}{\|\mathbf{v}\|^2}\mathbf{v} \tag{2.1}$$

$$\frac{1}{R} = \frac{\|\mathbf{a_n}\|}{\|\mathbf{v}\|^2} \tag{2.2}$$

As a validation of this method, a discrete calculation of spatial curvature is performed, taken from Bergou [44]; it is found that the two methods displayed identical trends but with different proportional scaling as a result of dimensional differences. The spline-differentiation method was kept because it retained a 1/m unit scale, which was useful for interpretation.

To achieve the discretized time series data necessary for entropy analysis, a straight-forward logarithmic binning strategy was employed. Bins ranges were logarithmically spaced from $10^{-1.3}$ to $10^{0.4}$ m^{-1}, these values being representative of typical minima and maxima of the data set. Exceptional points that were less than $10^{-1.3}$ m^{-1} were grouped into the lowest bin. A plot depicting this binning strategy is shown in Figure 2.4 and the resulting probability distributions used in entropy calculations are shown in Figure 2.5.

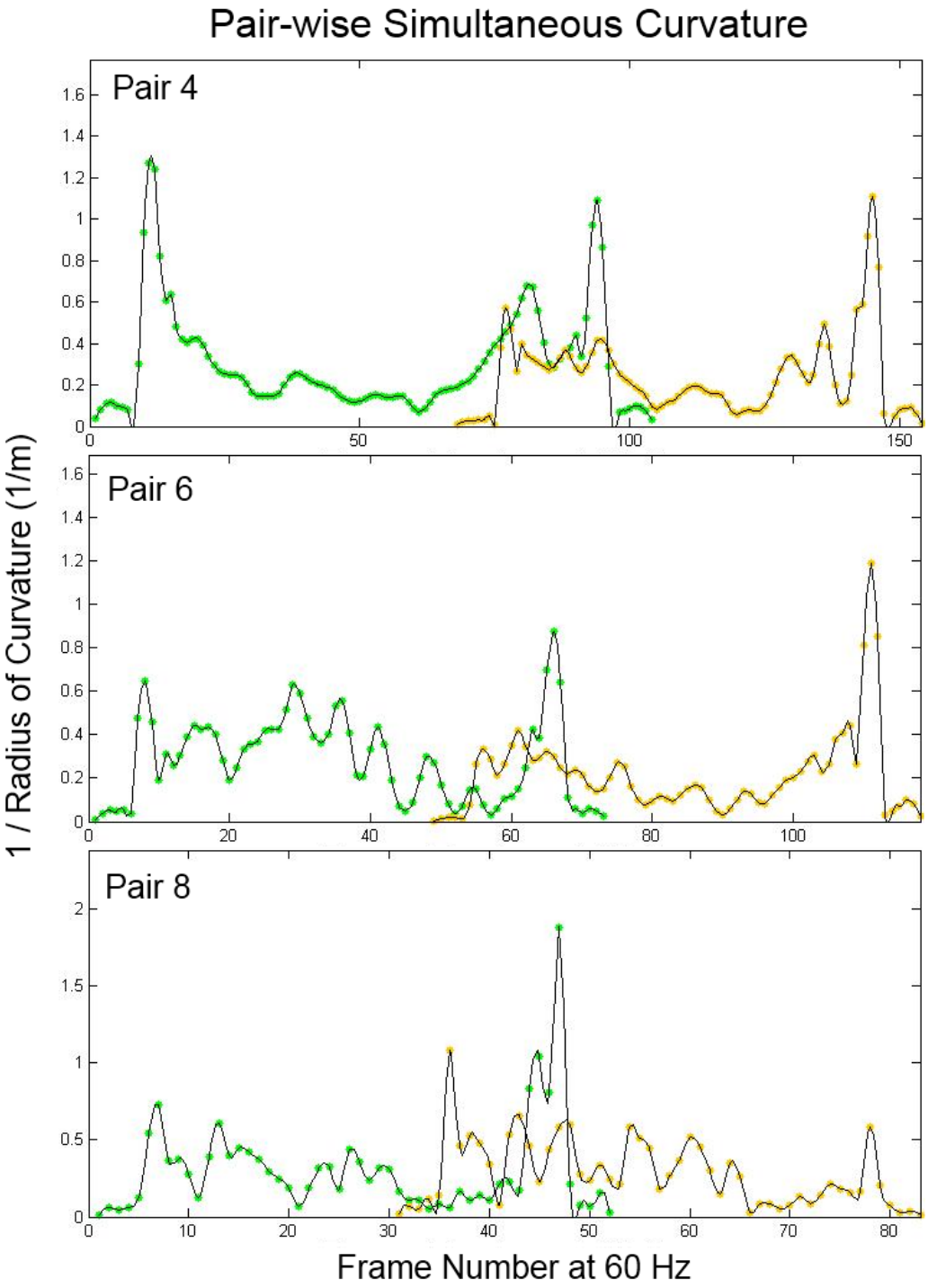

Figure 2.3: Sample pair-wise inverse curvature time series occurring in real time, as per the camera frame number. The green curve represents the front bat and the yellow curve the rear bat. It is critical to note, again, the similarity in shape. The time-delay, demonstrated by the x-axis displacement between each curve pair, can be accounted for with the modified transfer entropy formulation.

2.3 Transfer Entropy Approach and Hypothesis Proving

To prove the hypothesis of path coupling, a transfer entropy analysis of the inverse curvature data is performed. With a one-dimensional, discretized time series, a straightforward Shannon transfer entropy formulation [32, 45] is first applied. Shannon entropy, conditional entropy and free information are given by Equations (2.3), (2.4) and (2.5) respectively.

$$H(\mathbf{x}) = -\sum_{\mathbf{x}\in A} p(\mathbf{x}) \log p(\mathbf{x}) \tag{2.3}$$

$$H(\mathbf{x}|\mathbf{x_p}) = -\sum_{\mathbf{x},\mathbf{x_p}\in A} p(\mathbf{x},\mathbf{x_p}) \log p(\mathbf{x}|\mathbf{x_p}) \tag{2.4}$$

$$H(\mathbf{x}|\mathbf{x_p},\mathbf{y_p}) = -\sum_{\mathbf{x},\mathbf{x_p},\mathbf{y_p}\in A} p(\mathbf{x},\mathbf{x_p},\mathbf{y_p}) \log p(\mathbf{x}|\mathbf{x_p},\mathbf{y_p}) \tag{2.5}$$

The set A represents the possible discrete values of $\mathbf{x}$ and $\mathbf{y}$, as determined by the number of bins k, such that $A = \{a_1, a_2, ...a_k\}$. The vector $\mathbf{x} = \{x_1, x_2, ...x_N\}$ represents any of the potential discrete values along $t = \{t_1, t_2, ...t_N\}$ of the curvature signal receiving entropy, while $\mathbf{x_p}$ represents any value preceding a specific $\mathbf{x}(t)$ in the previous timestep. Similarly, $\mathbf{y_p}$ represents any value preceding a specific $\mathbf{x}(t)$ in the previous timestep, but from the entropy source curvature signal.

The function $p(\mathbf{x})$ represents the probability distribution of $\mathbf{x}$, determined by the frequency of a symbol ($a_i \in A$) appearing in the $\mathbf{x}$ time series. The distributions $p(\mathbf{x},\mathbf{x_p})$ and $p(\mathbf{x}|\mathbf{x_p})$ represent the digram and transitional probability distributions, respectively, of the $\mathbf{x}$ time series. Similarly, $p(\mathbf{x},\mathbf{x_p},\mathbf{y_p})$ and $p(\mathbf{x}|\mathbf{x_p},\mathbf{y_p})$ represent the digram and transitional probability distributions, respectively, of the $\mathbf{x}$ time series, with knowledge of the $\mathbf{y}$ time series.

In this way, conditional entropy indicates the total information of $\mathbf{x}$ given the previous values of $\mathbf{x}$, while free information represents the information of $\mathbf{x}$ given the previous values of $\mathbf{x}$ and $\mathbf{y}$. Thus, transfer entropy can be calculated in Equation (2.6), where transfer entropy is the information of $\mathbf{x}$ coming from previous values of $\mathbf{y}$ but not previous values of $\mathbf{x}$.

$$TE(\mathbf{y} \to \mathbf{x}) = H(\mathbf{x}|\mathbf{x_p}) - H(\mathbf{x}|\mathbf{x_p},\mathbf{y_p}) \tag{2.6}$$

Inherent in this formulation is the assumption of a 1st order Markov process [32], in which current values of a signal are only affected by the values of one time step prior. In accordance with the properties of this assumption, a number of important concepts are developed.

First, curvature data must be intelligently sampled such that a stimulus-response cycle can occur within a single timestep. If the bats are not capable of observing and adjusting their trajectory within a single timestep, positive results cannot be expected. This is resolved with a characteristic time scale argument later in this chapter.

Secondly, if interaction is delayed (in that a bat is capable of making a trajectory adjustment in a single timestep, but waits until later timesteps to do so), a traditional 1st order Markov formulation will not produce positive results. Based on the path coupling hypothesis and the time delay seen in the simultaneous inverse curvature plots, an interaction delay of this kind is anticipated. This led to the development of a method for addressing and capturing this potential phenomena.

Hence, a modified 1st order Markov process is proposed. The calculation of free information in Equation (2.6) is adjusted such that $\mathbf{y_p}$ can encapsulate not just the value of the entropy source signal corresponding with the preceding time step $(t-1)$, but a time step further back $(t-n$, where $n \geq 1)$. This formulation maintains the Markovianity of the process because the entropy recipient can still only refer to a single previous state of the entropy source, though that state is now n time steps preceding, instead of just one time step preceding. Conceptually, this is equivalent to a bat detecting an important change in his partner's path immediately, but consistently waiting until a later time step to incorporate that change, as would be the case for a bat that is attempting to follow another bat that is substantially ahead (in front). The final process is similar to methods for studying time-delayed dependencies that have been developed in well-established literature [35]. Figure 2.4 serves to illuminate the function of the modified Markov process. Additionally, a plot of the effect of n on a single transfer entropy calculation is shown in Figure 2.6.

With this modified formulation, an additional variable is created in the calculation of transfer entropy, n. To visualize the interactions of all three variables (number of bins, sample rate, and n shift value), one can plot a 2D transfer entropy map that varies sample rate and n shift. These maps can be generated for any number of bins, any pair, and any direction of interaction. Some samples of these maps are shown in Figure 2.7.

This huge array of transfer entropy data can be hazardous. Because results can depend strongly on the interpretation used, there are many opportunities for spurious conclusions to be reached [46]. In order to compose a supportable argument, physical reasonable sample rate, number of bins, and time delay values are selected , such that they could be considered characteristic scales of the system. By doing this, one eliminates regimes of results that do not have physical meaning and the bias of selecting regimes that artificially provide the most positive results is avoided. This form of interpretation argument is generally well-founded and can be demonstrated in the analysis performed by Butail on fish-robot interactions [40].

Given that an average wing-beat frequency for bats of the size observed is 10 Hz [7] and that one can reasonably assume a bat is capable of making trajectory adjustments four times per wing-beat, 40 Hz is selected as a best guess of a physical characteristic time scale. This also addresses the issue of insufficient stimulus-response cycle time, mentioned previously.

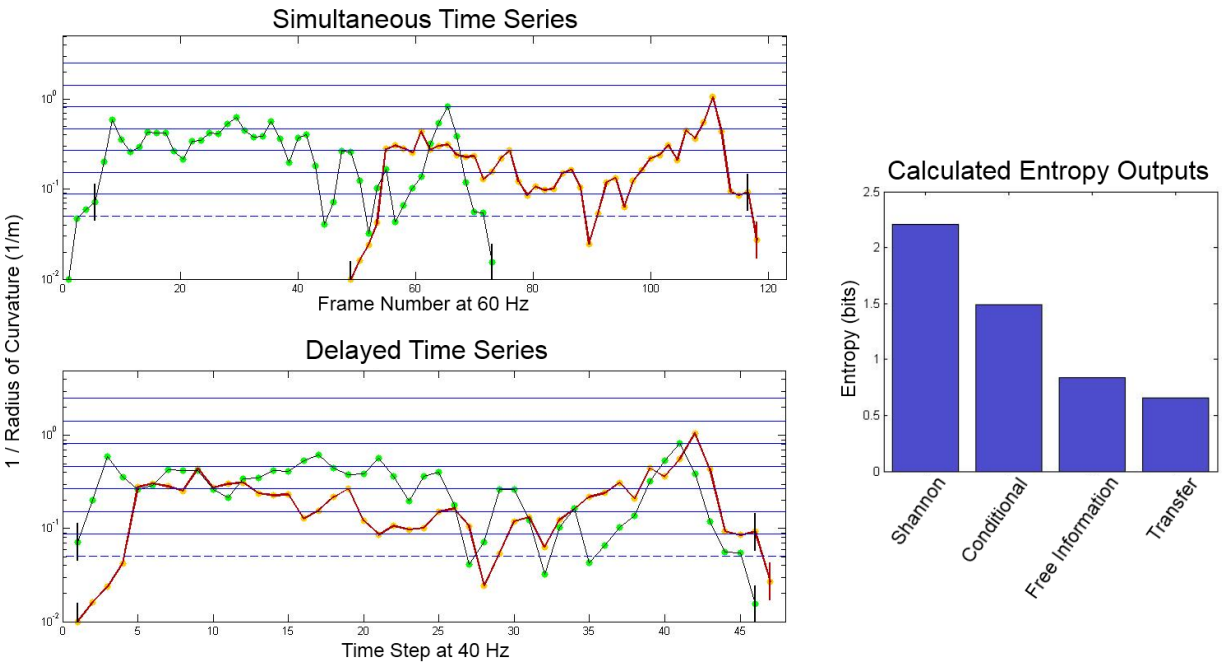

Figure 2.4: Depiction of modified Markov process. The top plot displays the original curvature time series from Figure 2.3, having been down-sampled (sub-frame timing is applied as necessary) and placed on a log scale. The lower plot displays the truncated and shifted time series with respect to the locally defined time step. In both plots, the green dot signal represents front bat and the yellow dot signal the rear bat. The signal highlighted in red is the entropy recipient, $\mathbf{x}$, for which the entropy values are being calculated; in this case, the entropy recipient is the rear bat. The non-highlighted signal is the entropy source, $\mathbf{y}$. Blue horizontal lines represent the minimum of each binning zone, eight in total. The lowest line is dashed since the lowest bin includes all values below its stated minimum. The unused bins have no effect on entropy calculations and are used by other pairs. The probability distributions generated by this example are shown in Figure 2.5. Looking at the entropy recipient, the red vertical line marks the final value of $\mathbf{x}$, while the black vertical lines mark the first and last value of $\mathbf{x_p}$. Similarly, looking at the entropy source, the black vertical lines mark the first and last value of $\mathbf{y_p}$, given the imposed n. Moving from the top plot to the bottom, the black vertical lines line up in time, indicating that these previously separated points (and all points in between) are being correlated in the calculation of free information $H(\mathbf{x}|\mathbf{x_p}, \mathbf{y_p})$, as per the modified formulation. All data presented here is sourced from Pair 6 at a sample rate of 40 Hz, $n = 30$ time steps. Though it is not relevant to the final analysis, for clarity, calculated entropy outputs for this example are included in the bar plot on the right.

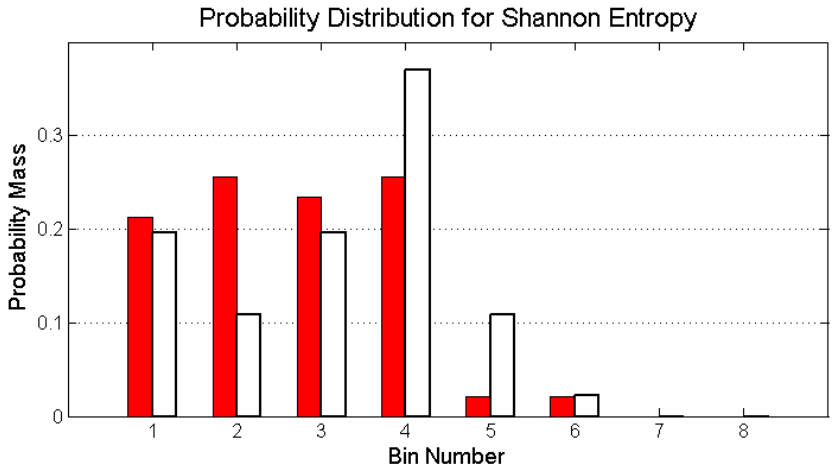

Figure 2.5: Sample plot of the probability distributions generated by the fixed logarithmic binning strategy employed on the curvature data, to be used in the calculation of Shannon Entropy. The red and white bars are the probability distributions of the **x** and **y** time series used in Figure 2.4.

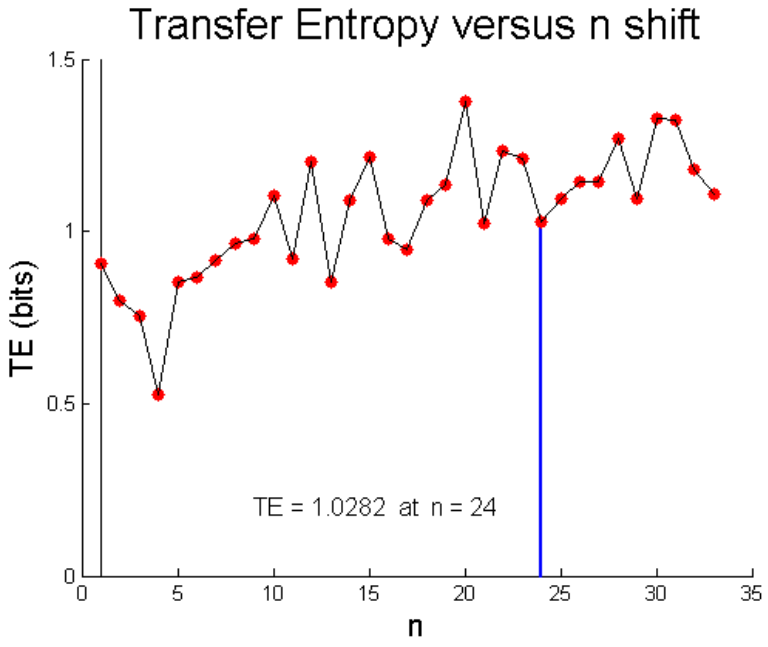

Figure 2.6: Sample plot of the general effect of n on transfer entropy. Generated from Pair 8 at 40 Hz with ten bins. The blue line represents the TE value of this data at $n = 24$, the n shift value calculated with the $\Delta t = 0.57$ value for Pair 8, using Equation (2.7).

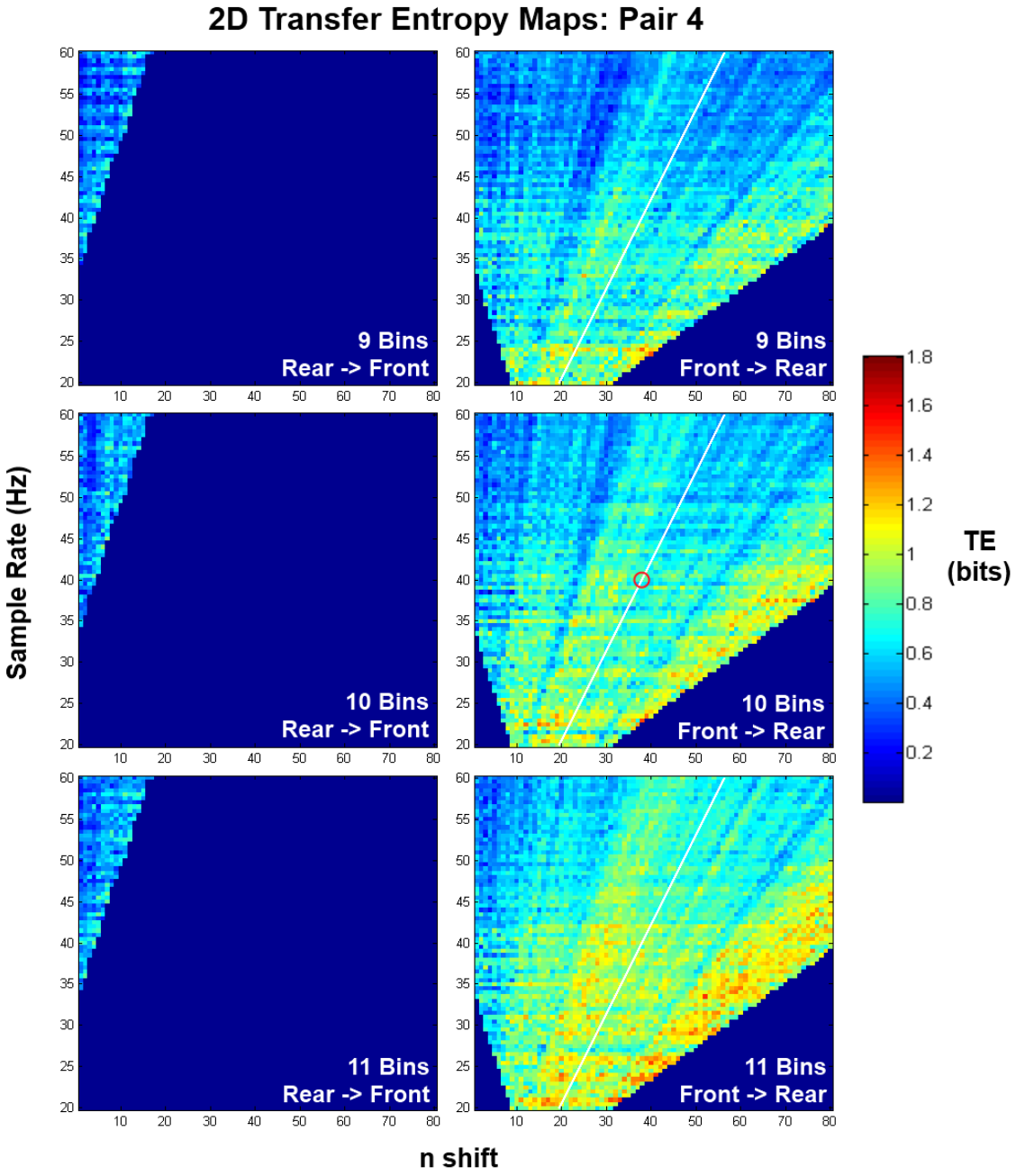

Figure 2.7: Sample of 2D transfer entropy maps. With axes of n shift and sample rate, variables such as pair number, directionality, and number of bins can be varied. Here, number of bins is varied from 9 to 11 considering both directions of information transfer in Pair 4. The thin white lines represent the Δt value for Pair 4 projected onto the front to rear maps using Equation (2.7). The three red circles indicate entropy values used in the final analysis. Plot areas of zero TE lack sufficient points for entropy analysis. Front to rear direction plots cover a broader plot area because n shift increases the number of common points between each signal in this case; the opposite is true for the rear to front direction.

Number of bins was selected as to allow a bat to easily move between bins within one time step[40], as well as to guarantee the performance envelope of the bat could be well captured. Ten bins was considered sufficient and thereby chosen.

For the n shift values, transfer entropy is first calculated with the conventional $n = 1$ to see the standard values. However, as previously mentioned, a time delay phenomenon correlating with path coupling is hypothesized. To capture this, a differential time factor (Δt) is calculated for each pair by dividing the average distance between the front and rear bat by the average velocity of the rear bat. This differential time factor represents the average time lag between when the rear bat sees the front bat at a particular location and when the rear bat achieves an equivalent location along its own path. Effectively, this delay incorporates path information from the front path at an equivalent point in space, rather than the previous point in time. If an increased value of transfer entropy is seen using this shift, it will serve as evidence for a path-coupling behavior from the front bat to the rear bat and a leader-follower interaction.

Precise differential time values are given in Table 2.1 and can be converted into n shift values with Equation (2.7), where SR is the chosen sample rate and rnd($\bullet$) rounds real numbers to the nearest integer.

$$n = \text{rnd}(\Delta t \cdot SR) + 1 \tag{2.7}$$

It is critical to note that this delay factor is inherently directional from the front bat to the rear. Given that the front bat is exclusively in front of the rear bat and cannot perceive stimuli from future time steps, imposing this same shift for the rear to front interaction would be entirely non-physical and would require using a negative n value.

Based on these properties, it is proposed that the front bat is only able to receive and incorporate path information from the rear bat based on the previous time step, as per a traditional 1st order Markov formulation, where as the rear bat can incorporate path information from front bat based on the previous time step or an equivalent point in space as per the $\Delta t \rightarrow n$ shift. This may seem to provide an unfair advantage to the rear bat, but this advantage appears to be inherent with nature of the system.

With all state variables decided, the final transfer entropies for each pair with each of these interaction modes are calculated to evaluate their respective presences. To clarify, the modalities considered are: $RF_{n=1}$, entropy from the rear to the front bat with $n = 1$, $FR_{n=1}$, entropy from the front to the rear bat with $n = 1$, and $FR_{\Delta t}$, entropy from the front to the rear bat with n determined by Δt.

In addition to these three modalities, a fourth value is added, representing a control condition, Modality Sh. Because there can be some amount of calculable information transfer between two time series that are entirely independent, calculated is a level of entropy present between curvature time series of bats that cannot possibly be interacting since they occupy the

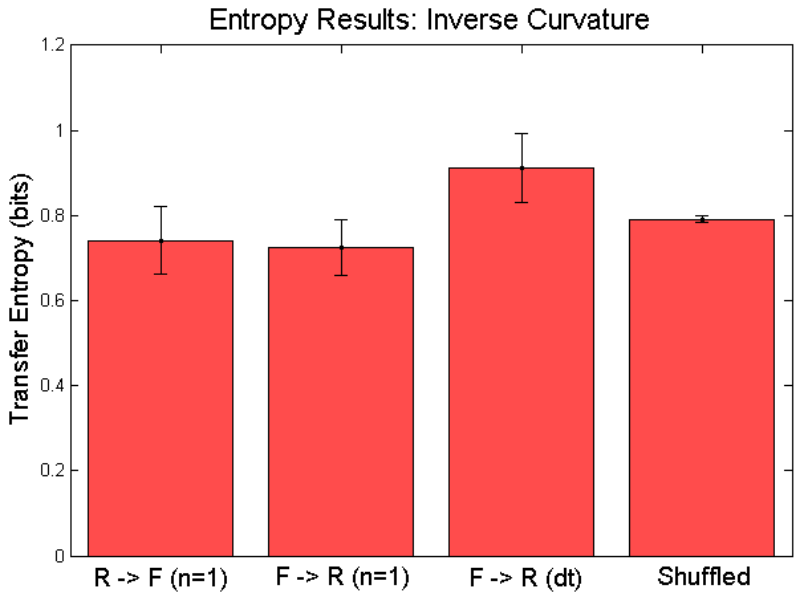

Figure 2.8: Final transfer entropy results for all pairs in each modality at a sample rate of 40 Hz and with ten bins. Red bars represent sample means and black brackets indicate standard error. $N = 10$ pairs are used for the first three modalities and $N = 1000$ samples for the shuffled control modality. No significant differences in means are present.

tracking volume at vastly different times . This is accomplished by randomly selecting 1000 sets of curvature time series, each set having an entropy recipient and source from different pairs, and calculating directional transfer entropy with a random n shift value. Ideally, this method can add validity to the results by representing a "background" level entropy that is systemic with the data and that other entropy levels can be compared to. Most importantly, matched pair modalities ($RF_{n=1}$, $FR_{n=1}$, and $FR_{\Delta t}$) need to exhibit higher levels of transfer entropy than the unmatched shuffled pair modality (Sh) in order to be considered significant.

2.4 Results

The results of this analysis can be seen in Figure 2.8. As evidenced by the figure, the mean value of the front to rear with imposed delay modality ($FR_{\Delta t}$) is higher than all other modalities, which are roughly equal. Using JMP 11 software, a one-way analysis of variance is performed to test the statistical significance of these trends. Using a typical significance level of $p < 0.05$, unfortunately, no main effect of modality on the mean transfer entropies is found.

With a Tukey-Kramer HSD test performed for post-hoc, pairwise tests (JMP 11), tests comparing Modality $FR_{\Delta t}$ to Modalities $RF_{n=1}$, $FR_{n=1}$, and Sh have lower p values (0.30,

0.38, 0.44, respectively) than all other pairs (0.77 for Sh to $FR_{n=1}$, 0.87 for Sh to $RF_{n=1}$, and 0.99 for $RF_{n=1}$ to $FR_{n=1}$). Although these tests fail to indicate statistical significance, the trend suggests that Modality $FR_{\Delta t}$ is the most dominant modality of directional information transfer in the system. This is to say, one finds highest information transfer from the bat flying in front to the bat flying in the rear while considering the path coupling time delay. This serves as reasonable evidence for a number of critical points: 1) relative spatial positioning plays an important role in navigational leadership, 2) the front bat in particular fulfills a leadership role for the pair as a whole, and 3) the rear bat displays path coupling behavior with the leading bat.

2.5 Discussion

Given the statistical non-significance of these results, one cannot conclusively determine the dominant leadership structure of the bats observed. Despite this, the general conclusions reached mesh very well with predictions drawn from literature. Given our understanding of cessation in bat echolocation [28] and information cascades in swarming simulations [43], a position-based leadership structure with path coupling appears highly probable, lending some legitimacy to these conclusions. It is suspected that in future studies with a larger sample size of pairs, the lack of significance encountered may be rectified and a leadership structure can be clearly defined.

As mentioned in earlier parts of this chapter, transfer entropy analyses are performed on tangential acceleration and total acceleration metrics, alternatives to the inverse curvature metric focused on. Though the data preparation section of this chapter detailed why these metrics are not the best representations of bat motion or the best candidates for entropy calculations, the analyses of these metrics are fundamentally identical to the analysis of the inverse curvature metric; the only difference is a centered, linearly-spaced binning strategy for the alternative metrics rather than a fixed logarithmic strategy. Results for the tangential acceleration and total acceleration metrics are shown in Figure 2.9. It is found that TE values are consistently lower and trends are less noticeable than in Figure 2.8, making these results less useful in addition to being less reliable. Given these observations, focus is rightfully put on the application and results of the inverse curvature metric.

Given the nature of transfer entropy calculations, the method employed for discretizing a continuous variable can have significant effects on the final output. In particular, results are often highly sensitive to the number of bins used to discretize. The Data Collection and Preparation section of this chapter detailed how curvature data is discretized with a fixed logarithmic binning strategy and the Transfer Entropy Approach and Hypothesis Proving section detailed the reasoning behind the choice of ten bins. However, it remains to be seen if the final results of our analysis (given by Figure 2.8) are sensitive to the selection of bin number. To resolve the uncertainty created by this concern, the final four-mode results using 10 bins are plotted against that of using 8, 9, 11, and 12 bins, shown in Figure 2.10. Given

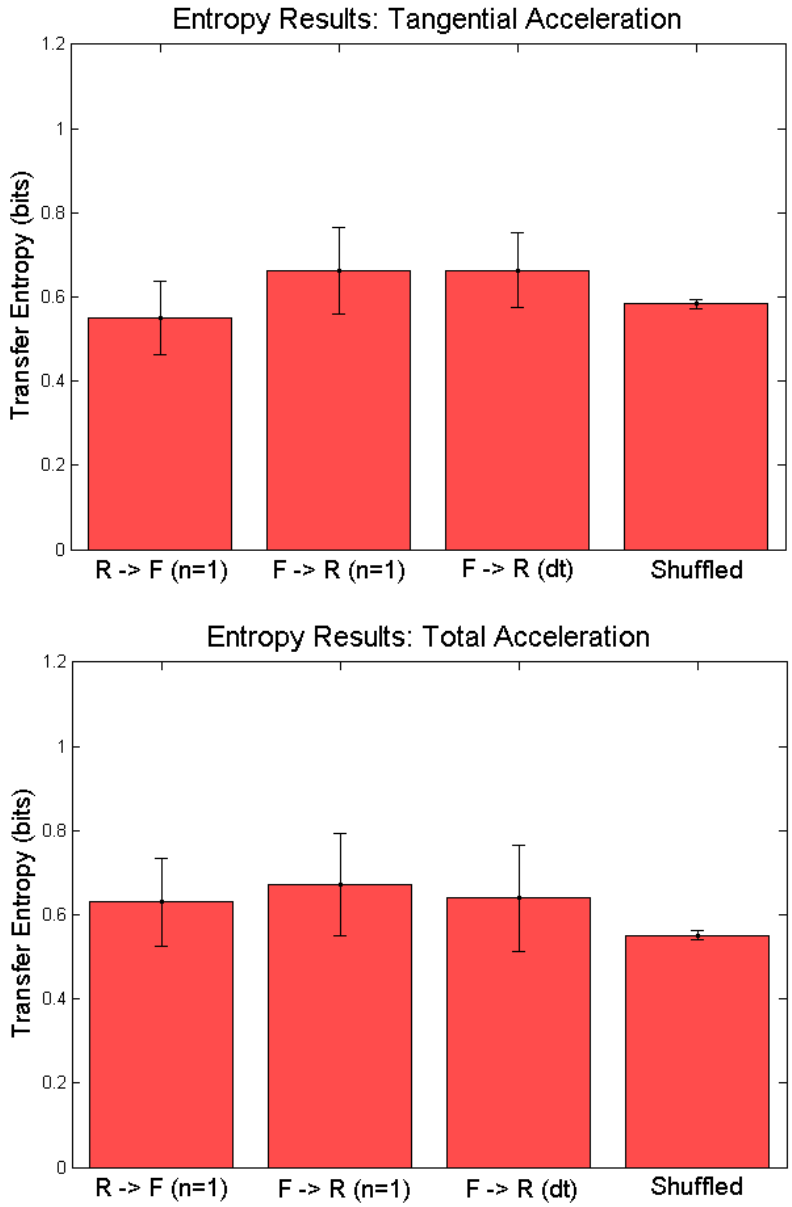

Figure 2.9: Final transfer entropy results using alternative metrics. Conditions are identical those of Figure 2.8: all pairs and modalities have a sample rate of 40 Hz and ten bins. Red bars represent sample means and black brackets indicate standard error. $N = 10$ pairs are used for the first three modalities and $N = 1000$ samples for the shuffled control modality.

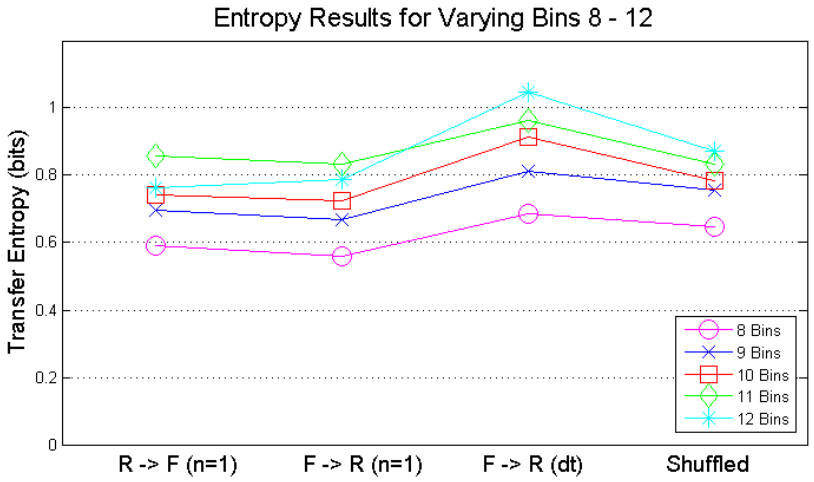

Figure 2.10: Binning sensitivity plot for transfer entropy calculations using curvature data at 40 Hz. Though average transfer entropy tends to increase with an increased number of bins, the inter-modal trends are quite stable. This provides good evidence that sensitivity to number of bins is not an issue in the results presented in Figure 2.8.

that the inter-modal trends shown in this plot are stable when we perturb the number of bins, no evidence is found that suggests the results in Figure 2.8 are sensitive to the number of bins chosen.

Concerns over the accuracy of the 3D data can be addressed with the details present in the previous chapter describing the development of the camera system. Additionally, the effects of small, or even sizable spatial inaccuracies would not have demonstrable effects on the comparison of kinematic time series. Bats within a pair are tracked through roughly the same volume of space, so any 3D spatial error entrenched in the camera system would be present in both time series, thereby being rendered null when comparisons between the time series are made for entropy analysis.

A significant weakness of this analysis lies in the brevity of the curvature signals. The mathematics of transfer entropy creates a cardinality issue when time series of very short length are analyzed. Calculations of free information must be fed signals consisting of a sufficiently large number of points in order to properly populate all probability distributions and avoid biased results [45, 47]. Though areas of highly erratic transfer entropy results are avoided by staying in timing regimes with relatively large series of points and contributions from anomalous entropy calculations are not seen, it remains arguable that the curvature time series need to contain more points in order for the transfer entropy analysis to be considered reliable.

An adaptable Bayesian binning strategy [47] may provide a solution by reducing the number of bins necessary to capture the behavior of a time series, thereby reducing the cardinality

and sparseness. Applying a Dirichlet distribution can reduce the effects of sparseness and regularize the probability distributions, as detailed in [45], though this can come at the cost of less significant results. More directly, an improved data collection method can serve to increase the total number of points. Expanding the tracking volume allows for an increased path length and thereby, more opportunities for interaction and information transfer, as well as a greater total number of points comprising each time series. In addition, more creative solutions may exist, such as performing cross-pair stitching to achieve representative front and rear bat signals while multiplying the total number of points. Future work with these ideas is likely to improve the validity and significance of results.

Appended to this document as Figures 2.11 through 2.20 are plots of the original 3D data of the bat trajectory pairs. It is presented for the benefit of the reader in the interest of future study.

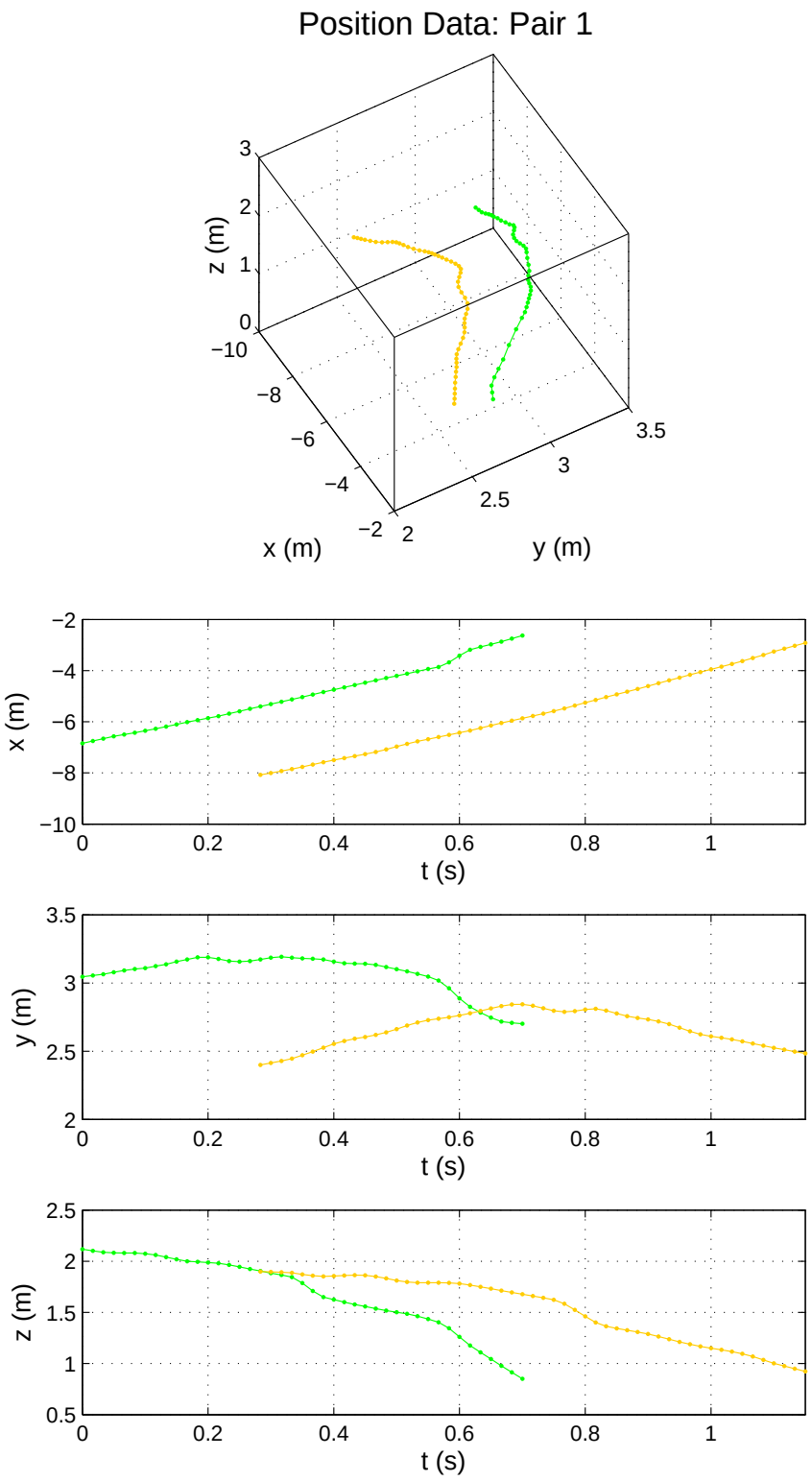

Figure 2.11: Raw 3D data for Pair 1.

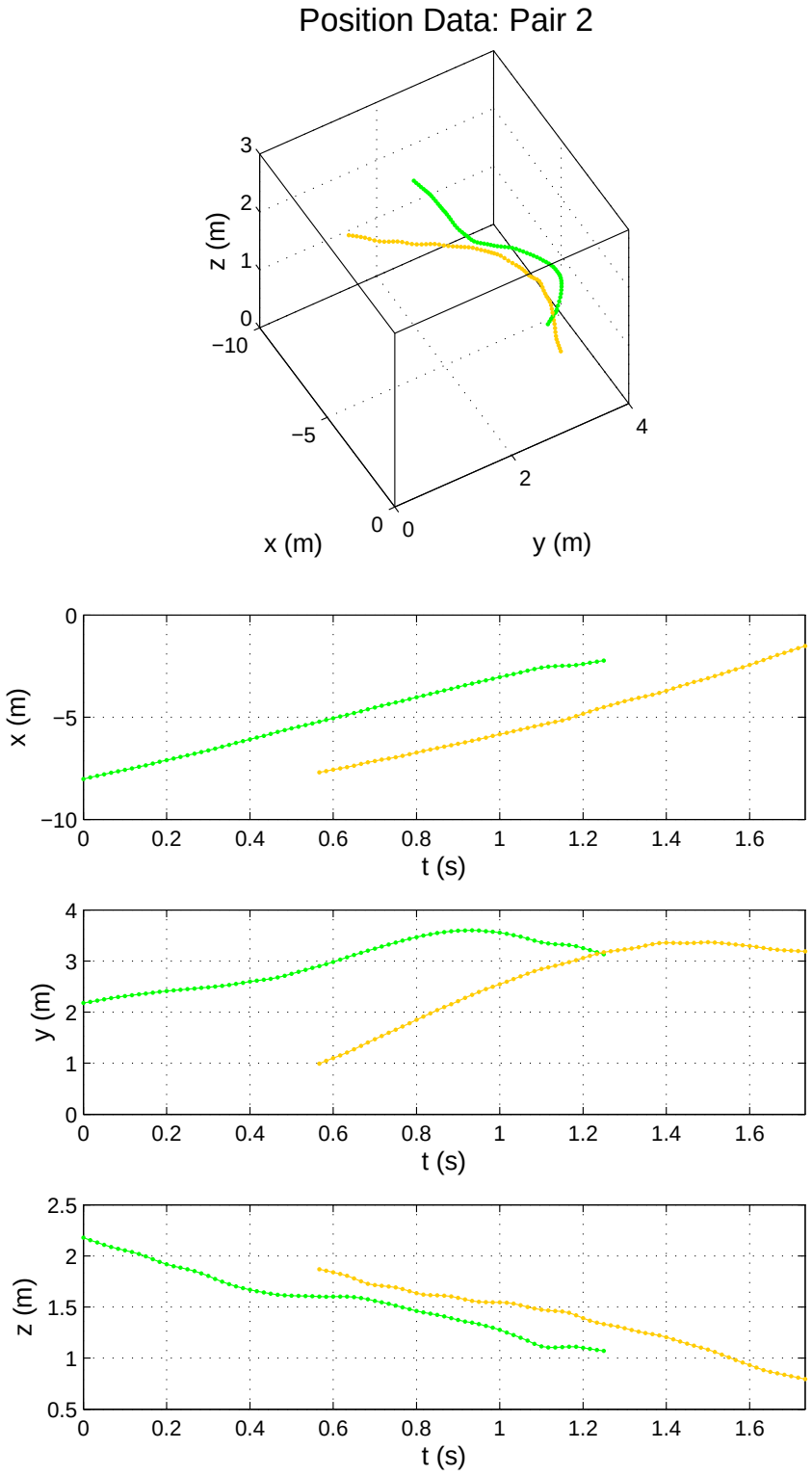

Figure 2.12: Raw 3D data for Pair 2.

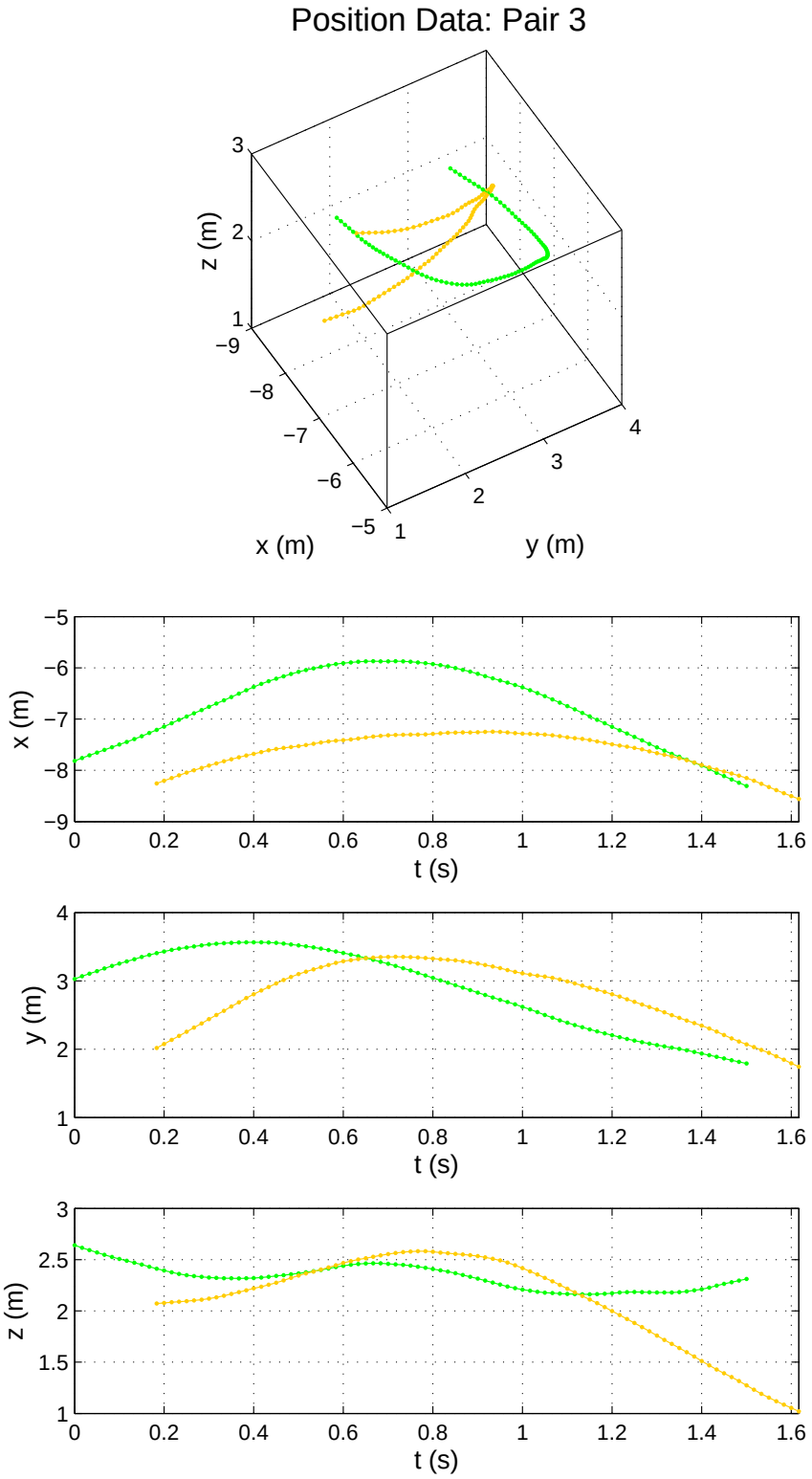

Figure 2.13: Raw 3D data for Pair 3.

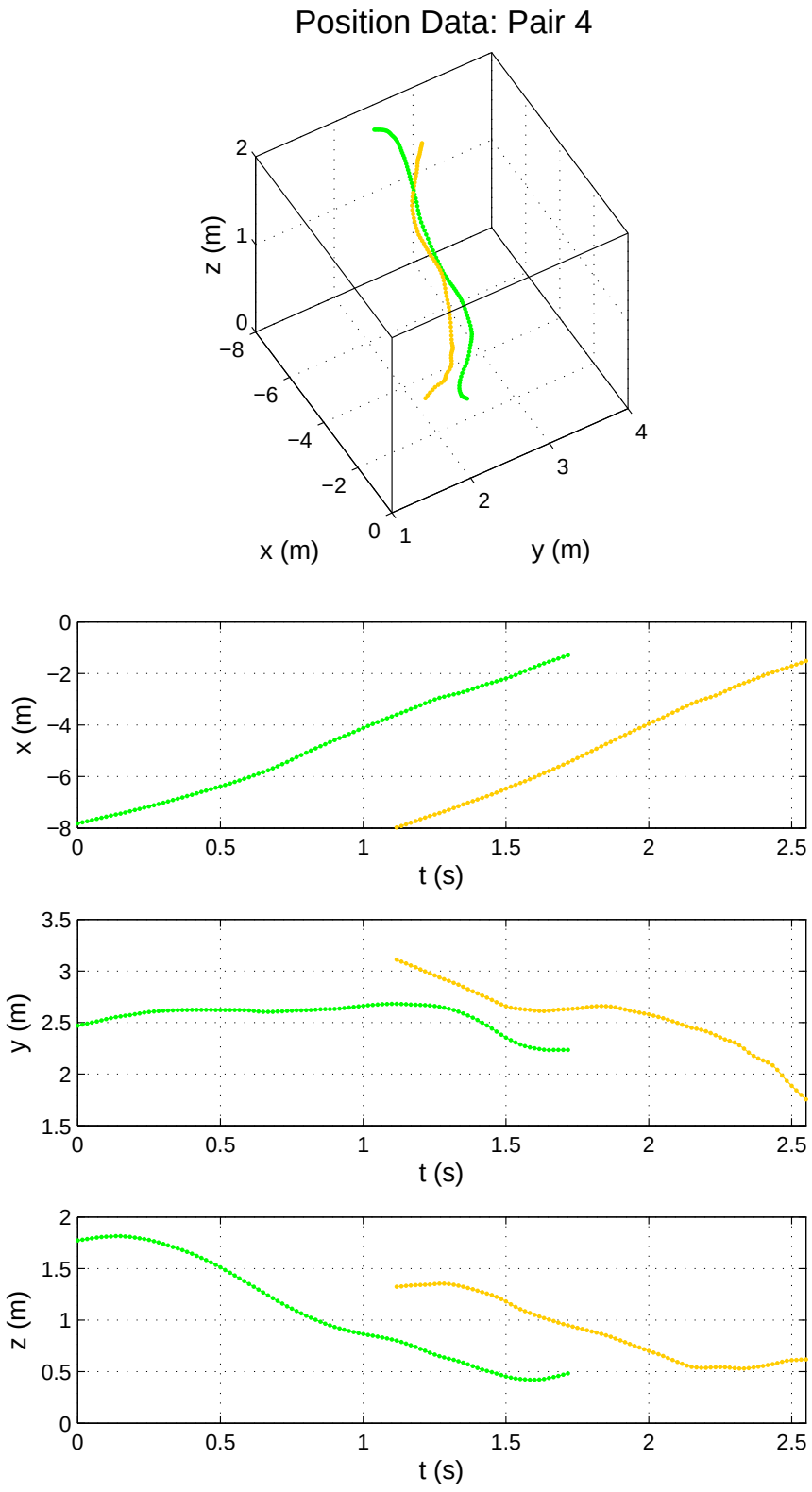

Figure 2.14: Raw 3D data for Pair 4.

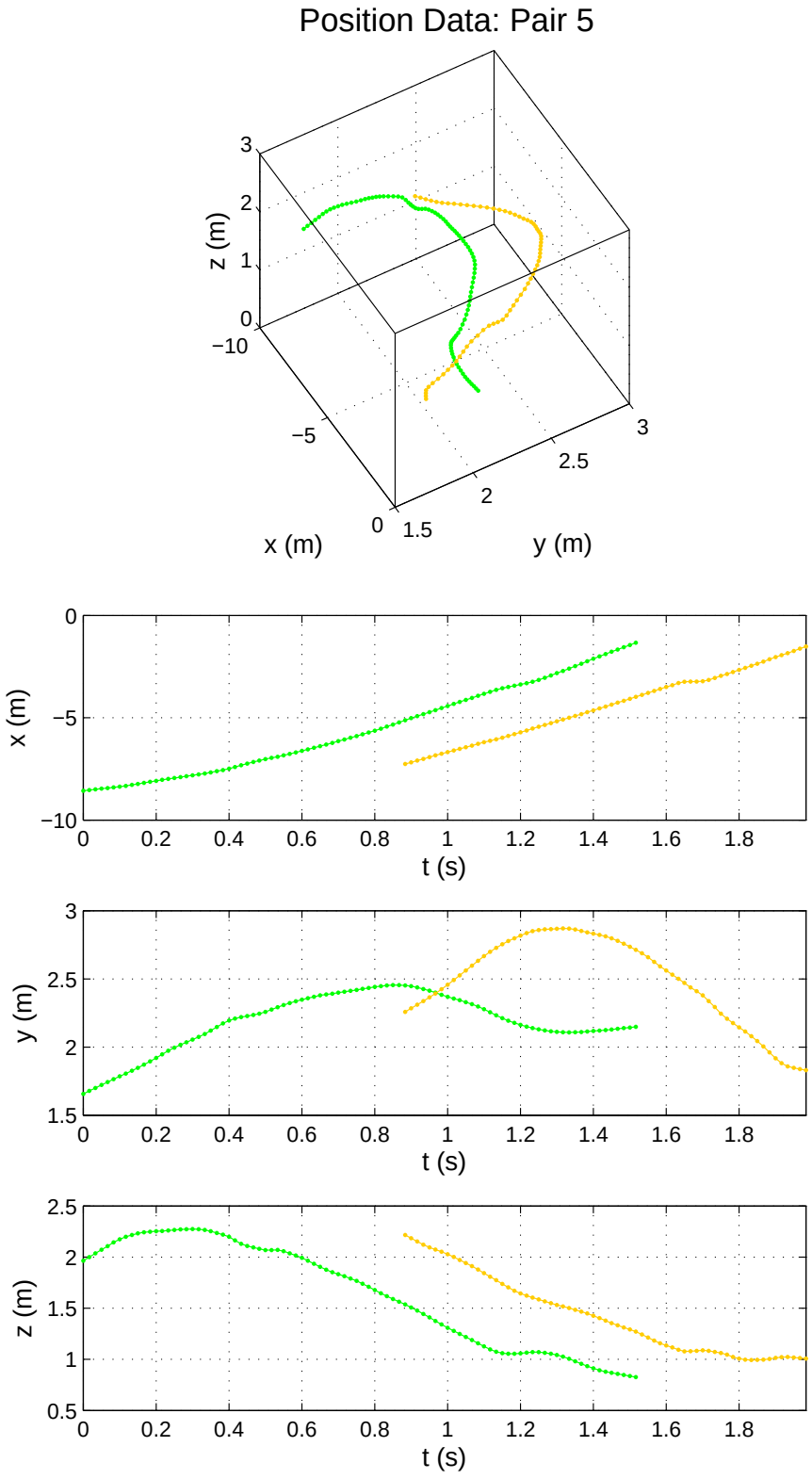

Figure 2.15: Raw 3D data for Pair 5.

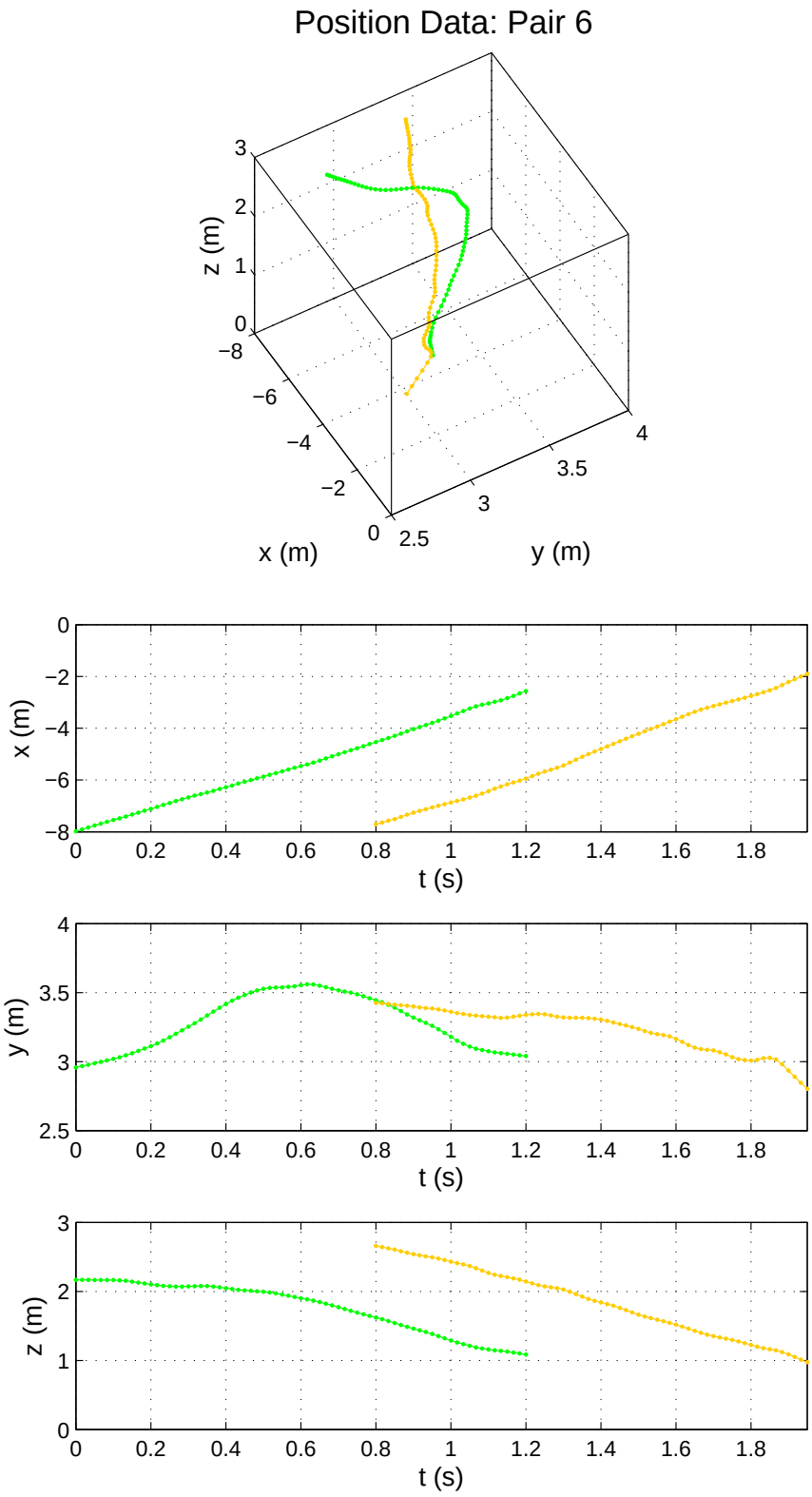

Figure 2.16: Raw 3D data for Pair 6.

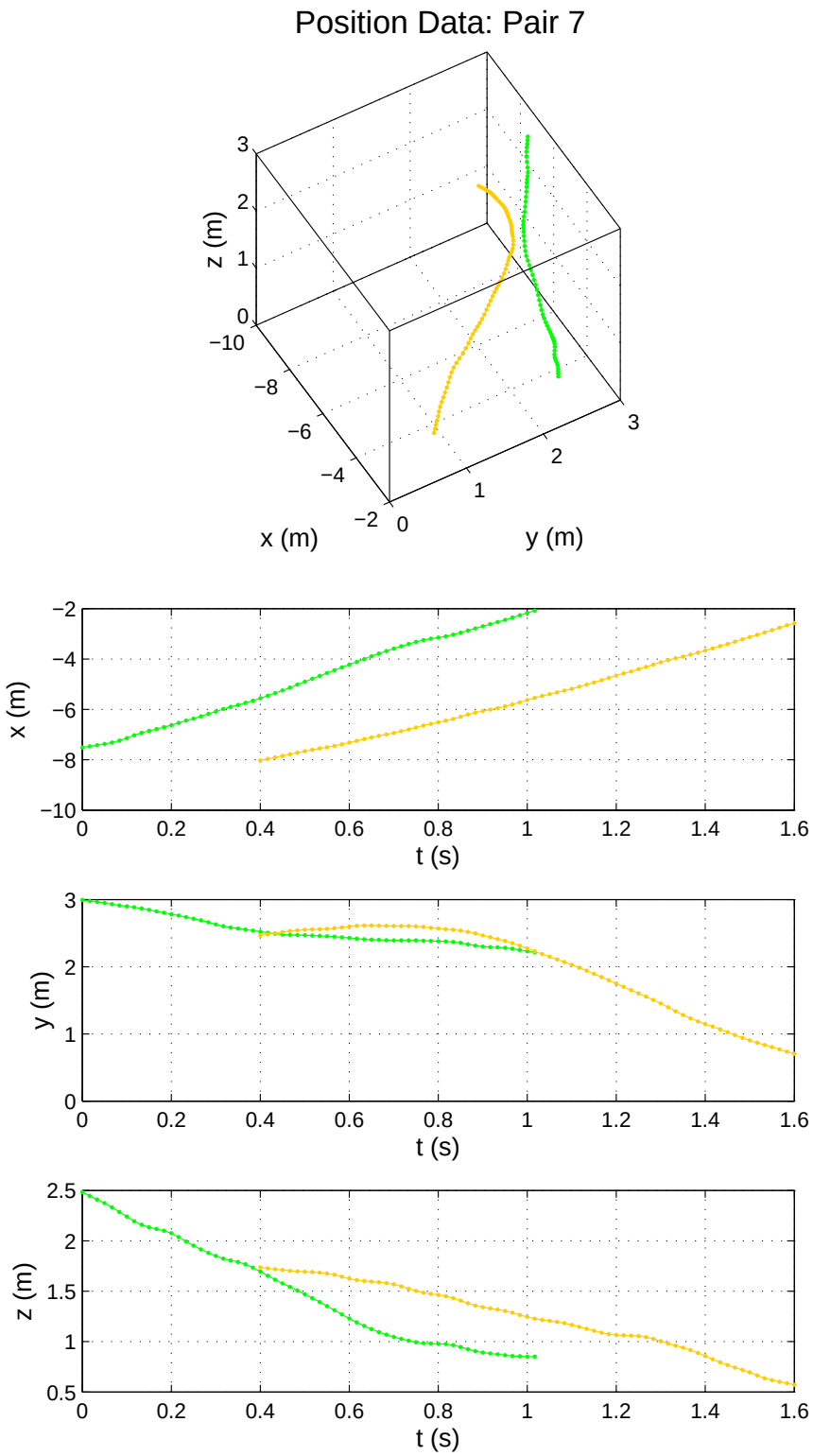

Figure 2.17: Raw 3D data for Pair 7.

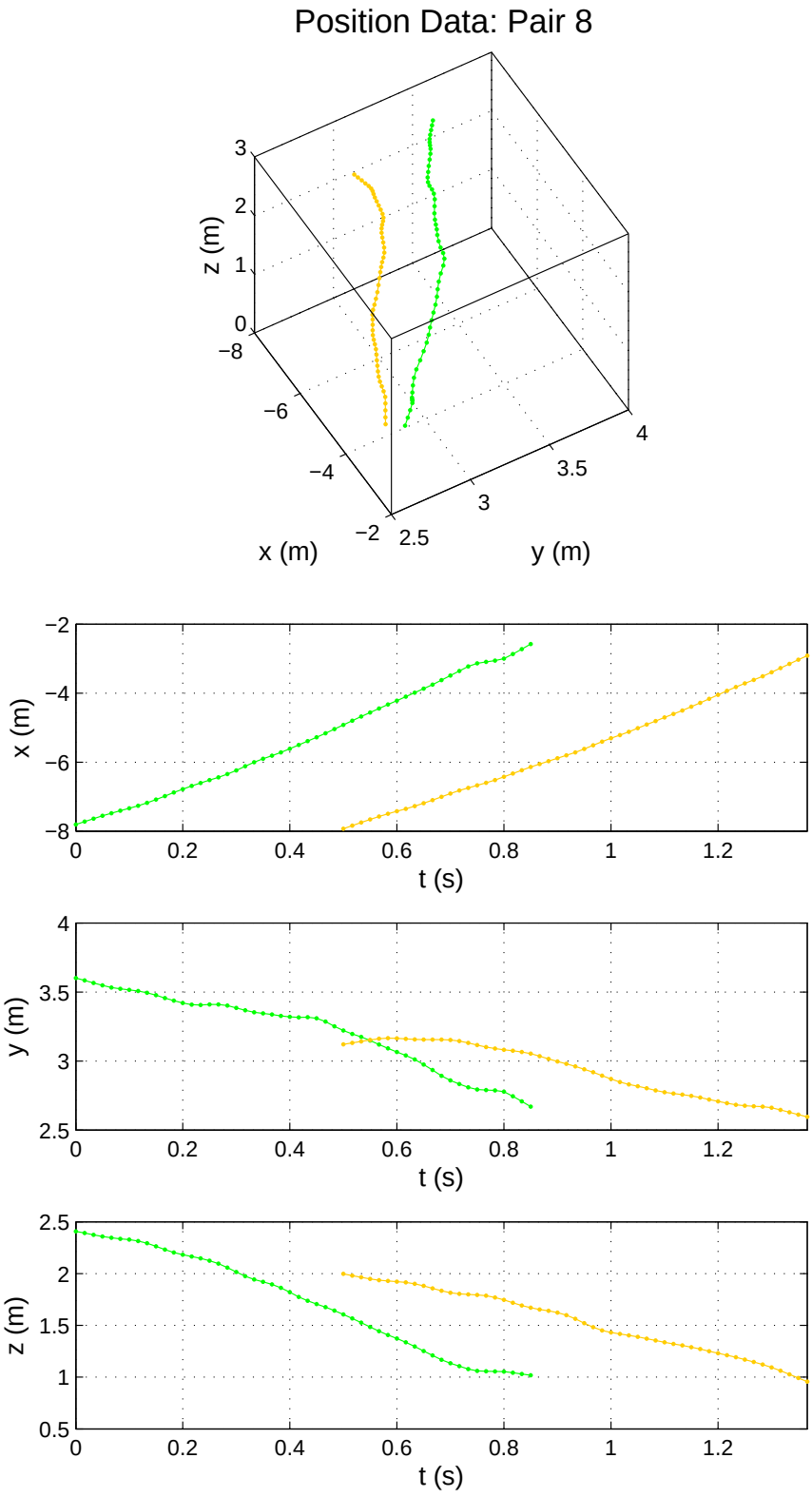

Figure 2.18: Raw 3D data for Pair 8.

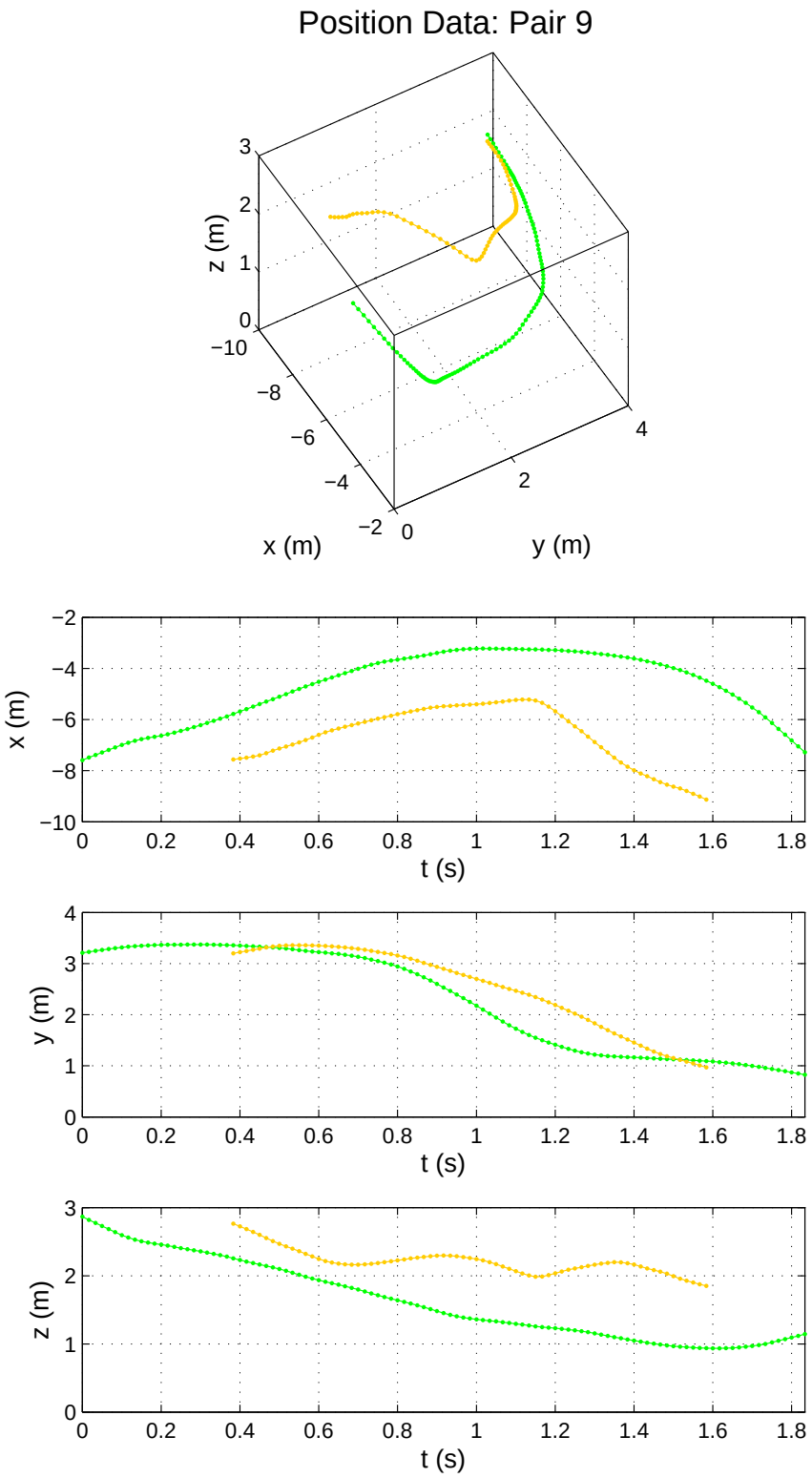

Figure 2.19: Raw 3D data for Pair 9.

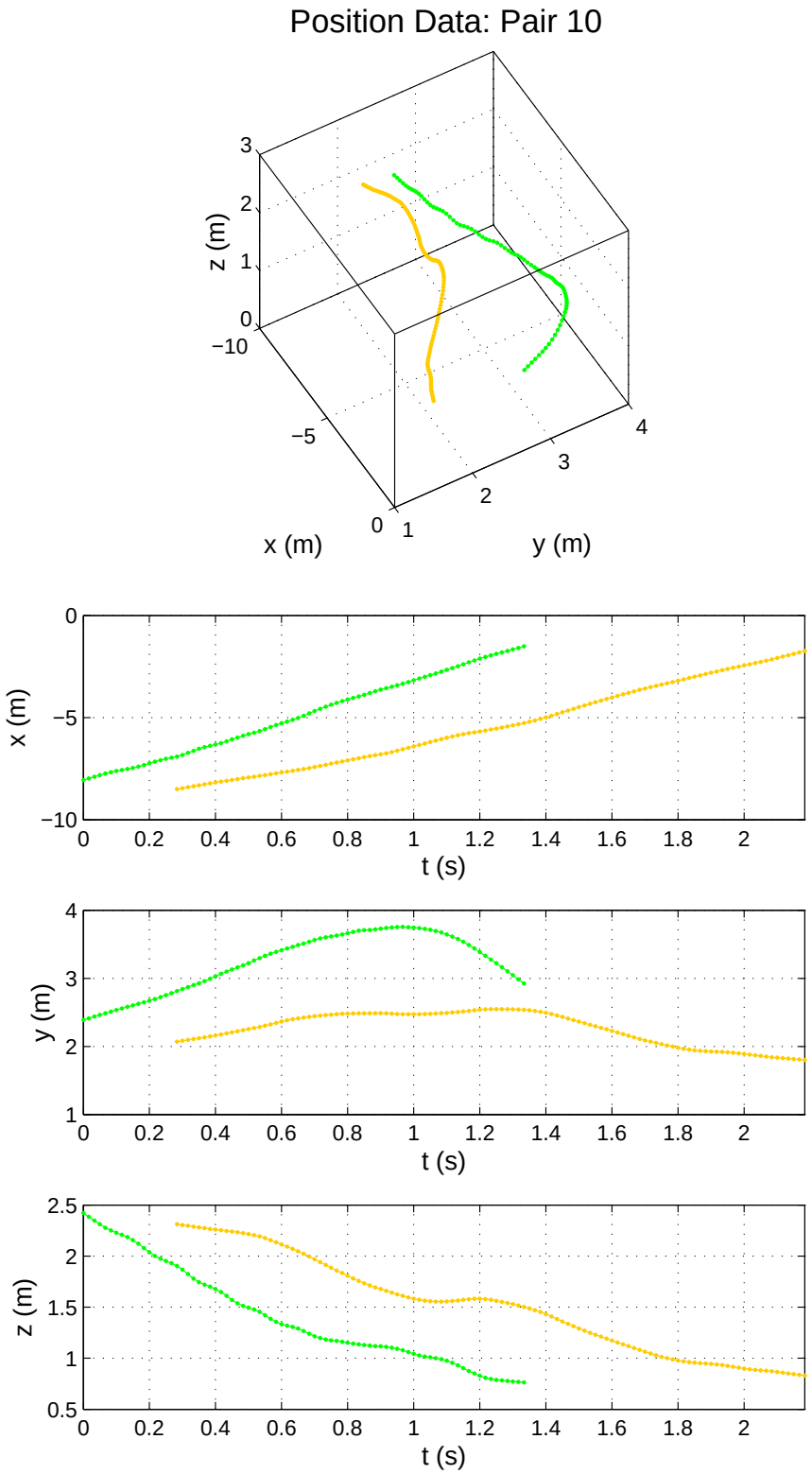

Figure 2.20: Raw 3D data for Pair 10.

Chapter 3

Bibliography

[1] Puckett, J. G., Kelley, D. H., and Ouellette, N. T., 2014. "Searching for effective forces in laboratory insect swarms". *Scientific Reports,* **4**.

[2] Shelton, R. M., Jackson, B. E., and Hedrick, T. L., 2014. "The mechanics and behavior of cliff swallows during tandem flights". *The Journal of Experimental Biology,* **217**(15), pp. 2717–2725.

[3] Hope, G., and Bhatnagar, K., 1979. "Electrical response of bat retina to spectral stimulation: comparison of four microchiropteran species". *Experientia,* **35**(9), pp. 1189–1191.

[4] Layne, J. N., 1967. "Evidence for the use of vision in diurnal orientation of the bat myotis austroriparius". *Animal Behaviour,* **15**(4), pp. 409–415.

[5] Bradbury, J. W., and Nottebohm, F., 1969. "The use of vision by the little brown bat, myotis lucifugus, under controlled conditions". *Animal Behaviour,* **17**, pp. 480–485.

[6] Theriault, D., Wu, Z., Hristov, N., Swartz, S., Breuer, K., Kunz, T., and Betke, M., 2010. Reconstruction and analysis of 3D trajectories of brazilian free-tailed bats in flight. Tech. rep., Boston University CS Department.

[7] Breslav, M., Fuller, N. W., and Betke, M., 2012. "Vision system for wingbeat analysis of bats in the wild". In Proceedings of the Workshop on Visual Observation and Analysis of Animal and Insect Behavior (VAIB 2012), Citeseer.

[8] Mann, A., 2009. *Infrared Optics and Zoom Lenses*. SPIE.

[9] Bernstein, D., 2011. *Essentials of Psychology*. Wadsworth.

[10] Feller, K., Lagerholm, S., Clubwala, R., Silver, M., Haughey, D., Ryan, J., Loew, E., Deutschlander, M., and Kenyon, K., 2009. "Characterization of photoreceptor cell types in the little brown bat myotis lucifugus (*vespertilionidae*)". *Comparative Biochemistry and Physiology Part B: Biochemistry and Molecular Biology,* **154**(4), pp. 412 – 418.

[11] Allen, E., and Triantaphillidou, S., eds., 2009. *The Manual of Photography and Digital Imaging*. Focal Press.

[12] IR-Pro, 2015. Hybrid wide night nir lens. http://www.ir-pro.com/choose-a-lens/hybrid-wide-night-ir-lens.

[13] Svoboda, T., 2011. Multi-camera self-calibration. http://cmp.felk.cvut.cz/~svoboda/SelfCal.

[14] Svoboda, T., Martinec, D., and Pajdla, T., 2005. "A convenient multicamera self-calibration for virtual environments". *PRESENCE: Teleoperators and Virtual Environments,* **14**(4), pp. 407–422.

[15] Bouguet, J.-Y., 2013. Camera calibration toolbox for MATLAB. http://www.vision.caltech.edu/bouguetj/calib_doc.

[16] Zou, D., Zhao, Q., Wu, H. S., and Chen, Y. Q., 2009. "Reconstructing 3d motion trajectories of particle swarms by global correspondence selection". In IEEE 12th International Conference on Computer Vision, pp. 1578–1585.

[17] Straw, A. D., Branson, K., Neumann, T. R., and Dickinson, M. H., 2011. "Multi-camera real-time three-dimensional tracking of multiple flying animals". *Journal of The Royal Society Interface,* **8**(56), pp. 395–409.

[18] Wu, Z., Hristov, N., Swartz, S., Kunz, T., and Betke, M., 2010. Tracking-reconstruction or reconstruction-tracking? Tech. rep., Boston University CS Department.

[19] Wu, Z., Hristov, N. I., Hedrick, T. L., Kunz, T. H., and Betke, M., 2009. "Tracking a large number of objects from multiple views". In IEEE 12th International Conference on Computer Vision, pp. 1546–1553.

[20] IR-Pro, 2011. Hybrid flat 5.5 night nir rectilinear lens. http://www.ir-pro.com/choose-a-lens/hybrid-flat-55-night-ir-lens.

[21] Xiao, F., and Wang, L., 2006. "State consensus for multi-agent systems with switching topologies and time-varying delays". *International Journal of Control,* **79**(10), pp. 1277–1284.

[22] Dudek, G., Jenkin, M. R., Milios, E., and Wilkes, D., 1996. "A taxonomy for multi-agent robotics". *Autonomous Robots,* **3**(4), pp. 375–397.

[23] Martinoli, A., Easton, K., and Agassounon, W., 2004. "Modeling swarm robotic systems: A case study in collaborative distributed manipulation". *The International Journal of Robotics Research,* **23**(4-5), pp. 415–436.

[24] Yang, X.-S., 2010. "A new metaheuristic bat-inspired algorithm". In *Nature Inspired Cooperative Strategies for Optimization (NICSO 2010)*. Springer, pp. 65–74.

[25] Jordehi, A. R., 2015. "Chaotic bat swarm optimisation (CBSO)". *Applied Soft Computing,* **26**, pp. 523–530.

[26] Ulanovsky, N., Fenton, M. B., Tsoar, A., and Korine, C., 2004. "Dynamics of jamming avoidance in echolocating bats". *Proceedings of the Royal Society of London B: Biological Sciences,* **271**(1547), pp. 1467–1475.

[27] Bates, M. E., Stamper, S. A., and Simmons, J. A., 2008. "Jamming avoidance response of big brown bats in target detection". *Journal of Experimental Biology,* **211**(1), pp. 106–113.

[28] Chiu, C., Xian, W., and Moss, C. F., 2008. "Flying in silence: echolocating bats cease vocalizing to avoid sonar jamming". *Proceedings of the National Academy of Sciences,* **105**(35), pp. 13116–13121.

[29] Corcoran, A. J., and Conner, W. E., 2014. "Bats jamming bats: Food competition through sonar interference". *Science,* **346**(6210), pp. 745–747.

[30] Getchell, A., 2008. "Agent-based modeling". *Physics,* **22**(6), pp. 757–767.

[31] Xiao, F., Wang, L., and Wang, A., 2006. "Consensus problems in discrete-time multiagent systems with fixed topology". *Journal of Mathematical Analysis and Applications,* **322**(2), pp. 587–598.

[32] Shannon, C., and Weaver, W., 1949. "The mathematical theory of information". *Urbana: University of Illinois Press.*

[33] Rényi, A., 1961. "On measures of entropy and information". In Fourth Berkeley Symposium on Mathematical Statistics and Probability, Vol. 1, pp. 547–561.

[34] Marko, H., 1973. "The bidirectional communication theory–a generalization of information theory". *IEEE Transactions on Communications,* **21**(12), pp. 1345–1351.

[35] Kaiser, A., and Schreiber, T., 2002. "Information transfer in continuous processes". *Physica D: Nonlinear Phenomena,* **166**(1), pp. 43–62.

[36] Schreiber, T., 2000. "Measuring information transfer". *Physical Review Letters,* **85**(2), p. 461.

[37] Dimitrov, A. G., Lazar, A. A., and Victor, J. D., 2011. "Information theory in neuroscience". *Journal of Computational Neuroscience,* **30**(1), pp. 1–5.

[38] Kwon, O., and Yang, J.-S., 2008. "Information flow between composite stock index and individual stocks". *Physica A: Statistical Mechanics and its Applications,* **387**(12), pp. 2851–2856.

[39] Ver Steeg, G., and Galstyan, A., 2012. "Information transfer in social media". In Proceedings of the 21st International Conference on World Wide Web, ACM, pp. 509–518.

[40] Butail, S., Ladu, F., Spinello, D., and Porfiri, M., 2014. "Information flow in animal-robot interactions". *Entropy,* **16**(3), pp. 1315–1330.

[41] Kadota, M., White, E. J., Torisawa, S., Komeyama, K., and Takagi, T., 2011. "Employing relative entropy techniques for assessing modifications in animal behavior". *PloS One,* **6**(12), p. e28241.

[42] Paulus, M. P., Geyer, M. A., Gold, L. H., and Mandell, A. J., 1990. "Application of entropy measures derived from the ergodic theory of dynamical systems to rat locomotor behavior". *Proceedings of the National Academy of Sciences,* **87**(2), pp. 723–727.

[43] Wang, X. R., Miller, J. M., Lizier, J. T., Prokopenko, M., and Rossi, L. F., 2012. "Quantifying and tracing information cascades in swarms". *PloS One,* **7**(7), p. e40084.

[44] Bergou, M., Wardetzky, M., Robinson, S., Audoly, B., and Grinspun, E., 2008. "Discrete elastic rods". In ACM Transactions on Graphics (TOG), Vol. 27, ACM, p. 63.

[45] Choi, H., 2014. "Localization and regularization of normalized transfer entropy". *Neurocomputing,* **139**, pp. 408–414.

[46] Smirnov, D. A., 2013. "Spurious causalities with transfer entropy". *Physical Review E,* **87**(4), p. 042917.

[47] Endres, D., and Foldiak, P., 2005. "Bayesian bin distribution inference and mutual information". *IEEE Transactions on Information Theory,* **51**(11), Nov, pp. 3766–3779.